MonoFlex: A 3D-Printed Non-Assembly Steerable Instrument

Graduation Thesis

Loes Bazuin

Delft University of Technology

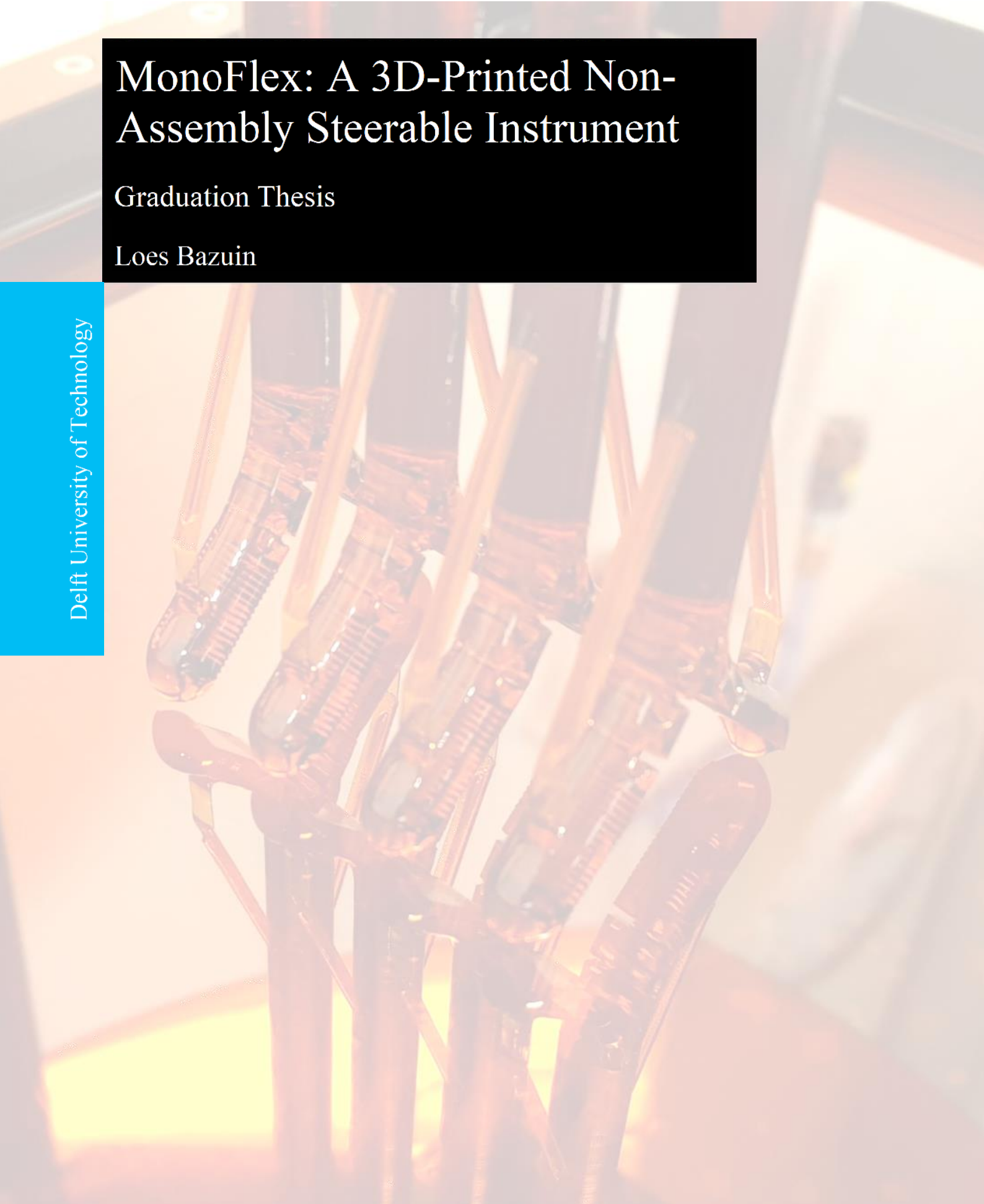

Supervisors: **Prof. dr. ir. P. Breedveld**
M.Sc. M. Scali
M.Sc. C. Culmone

TU Delft Delft University of Technology

Challenge the future

MonoFlex: A 3D-Printed Non-Assembly Steerable Instrument

By

G.P.L. Bazuin B.Sc. ME

in partial fulfilment of the requirements for the degree of

Master of Science
in Biomedical Engineering [BME]

at the Delft University of Technology,
to be defended on Wednesday the 27th of March, 2019 at 11:00.

Thesis committee:	Prof. dr. ir. P. Breedveld
	Dr. ir. J.F.L. Goosen
	M.Sc. M. Scali
	M.Sc. C. Culmone

Preface

The basis for this research originally lays in my passion for contributing to a better healthcare. In recent history, medical techniques and instruments are developed that enable quick recovery, less pain and little to no scars on the patient. It is my dream to invent and develop medical instruments to improve the health care even more for future generations.

I could not have achieved the end result of this research without a number of people supporting me. Firstly, I like to thank Remi van Starkenburg for his advice and help during all the printing iterations. He made all the designs ready to be printed, printed them, and performed the post-processing. He also gave me many tips when it comes to the optimization of the designs. Secondly, I want to thank Jos van Driel for his assistance during the final tests. I also want to thank my supervisors Marta Scali and Costanza Culmone for the time they made free for me during the process of fulfilling my thesis and testing the many parts that are 3D-printed. The many meetings really helped me during this period. Finally, I want to thank my parents, family, friends and last but not least, my fiancé, Ricardo, who supported and encouraged me during all the parts of my studies, and especially during the final months. Thank you all for your unwavering support.

Loes Bazuin

Cover photo is made by P. Breedveld, 2019

Abstract

The DragonFlex, world's first 3D-printed steerable Minimally Invasive Surgery (MIS) instrument, showing promising results for the medical field, is made by means of 3D-printing, and features simple assembly, while exhibiting high bending stiffness. In this research, the possibilities with additive manufacturing are explored even further, by minimizing the number of parts and thereby reducing the assembly time. The objective of the study was to design a one-part instrument, based on the DragonFlex, having the same functionality as the DragonFlex, while only requiring the assembly of the control wires. This one-part instrument is called the MonoFlex. In an iterative process of designing in SolidWorks (2018) and testing printed samples, the design of the MonoFlex was developed until final prototypes were obtained, both with and without steering segments. Final compression and torsion tests showed that the grasping forceps side and the control handle side, broke when exposed to torsion moments of 32.9 Nmm and 20.8 Nmm respectively and compression forces of 0.2 N and 1.5 N respectively. When the instruments were exposed to tensile forces up to 19.6 N, both sides did not show any sign of failure. The maximum grasping force reached was 2.4 N, lower that the average grasping forces (of 10 – 20 N), required to grasp tissue. The printed parts were slightly different from the parts drawn in SolidWorks, this was because of the incomplete addition of support material, and the post-processing method. The working principle of a one-part 3D-printed grasping prototype was proven. A recommendation for future research is to make the MonoFlex stronger and more durable by using multiple materials. This will bring medical technology another step closer to fully non-assembly 3D-printable MIS instruments.

Contents

MonoFlex: A 3D-Printed Non-Assembly Steerable Instrument

By

G.P.L. Bazuin

1. Introduction

1.1. Instruments for minimally invasive surgery.

Minimally invasive surgery (MIS) was introduced to reduce the negative effects of open surgery, such as long recovery time and large scars, by using very small incisions as entry points for the instruments [1-5]. During laparoscopy for example, trocars are accommodated in the small incisions in the abdominal wall and serve as airtight seals when the abdominal cavity is inflated with carbon dioxide, creating a working space for the clinician. Long and slender instruments can be inserted through the trocars, and provide the ability to visualize or manipulate tissues. These MIS instruments feature either a fully rigid or a steerable tip [6,7]. Rigid MIS instruments consist of a handle, a rigid shaft, and a tip, providing four degrees of freedom (DOF), namely axial sliding, axial rotation and pivoting in two perpendicular planes around the incision point (Fig. 1(a)) [8]. Since the incision point acts as a fulcrum, the motion of rigid instruments is considerably restricted and so is the clinicians approach to the tissue [2,7]. Therefore, rigid designs of MIS instruments were enriched with a steerable tip, adding two DOF, enabling the clinician to reach behind obstacles (Fig. 1(b)) [7-9].

1.2. DragonFlex.

One example of a steerable MIS instrument is the DragonFlex (Fig. 2), developed at Delft University of Technology (The Netherlands). The DragonFlex is a steerable MIS instrument prototype, designed to feature a steerable cable-driven joint construction free from fatigue, but with a high bending stiffness which is required for surgery [9-11]. The tip of the DragonFlex contains four parts, driven by two cables which are mechanically fixed in the handle. The tip enables joint articulation in two perpendicular planes and the grasper on the tip opens up to 180º. The instrument is produced by means of 3D-printing, featuring simple assembly while exhibiting high bending stiffness. The complete instrument with seven parts and two cables in the tip, shaft and handle, enables control of seven DOF. The DragonFlex concept shows that additive manufacturing could be a solution for medical instruments, as it is suitable for disposable use.

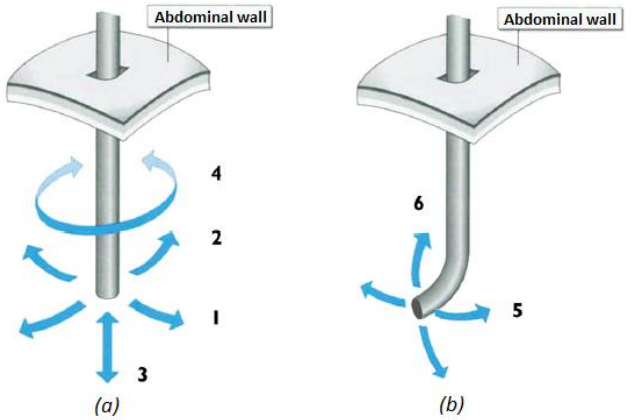

Figure 1: Degrees of freedom for different instruments. (a) Rigid instrument DOF [8], (b) additional steerable tip DOF [9].

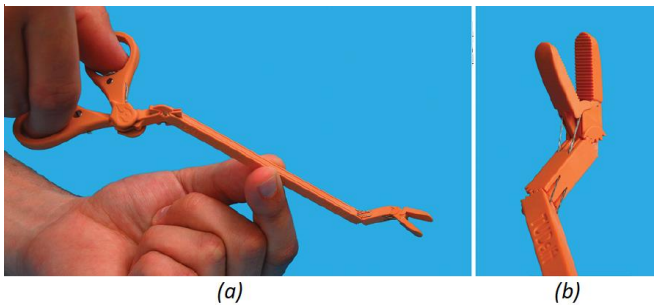

Figure 2: DragonFlex Prototype. (a) Complete instrument, (b) close-up on the tip showing cable-driven joints and grasping mechanism. Adapted from [9].

The printing technique used for the DragonFlex is VAT Photopolymerisation also called stereolithography (SLA) [12]. This type of additive manufacturing uses a vat with liquid polymer resin which is cured by ultraviolet light to form the parts. A platform on which the part to be printed is placed, moves upwards after curing of a new layer. In this way, the parts are built layer by layer. Different materials are used for the DragonFlex during the development of the instrument. One of prototype was printed with EnvisionTECVR NanoCure R5 resin [12], by the EnvisionTEC's Perfactory® 4 Mini XL with ERM. R5 is a relatively strong and hard polymer with high flexibility which made the DragonFlex tough and resistant. An advantage of this type of material is the transparency, making it possible to see the cable slots, which is useful during the testing phases. Because of the material properties and the promising results this material showed, the same material will be used during the design project described in this paper.

1.3. Problem definition.

The DragonFlex consisting out of seven printed parts and two cables is a breakthrough, showing that 3D-printing could be a solution for steerable MIS instruments, as it is suitable for disposable use. However, the possibilities with additive manufacturing could be explored even further, by minimizing the number of parts and thereby reducing the assembly time. The reason for minimizing the number of parts has mainly to do with production time and costs. Especially for instruments that are used regularly and are intended for disposable use, assembly time can be saved in the production process.

The DragonFlex is the world's first 3D-printed steerable MIS instrument prototype, giving promising results for the development of other surgical instruments. This study aims to prove that medical instruments, such as the DragonFlex, can be printed at once, not requiring assembly apart from the control cables. This would be highly useful for other medical applications and future development of other additive manufactured steerable instruments.

1.4. Objective

The goal of the study is to design a minimally assembly instrument with a non-assembly main body, having the same functionality as the DragonFlex, but which is easier to make, less time-consuming during the fabrication and low cost. This means it should be steerable, it should be able to grasp tissue, and it should be printable in one part. The focus will be on the design of printable joints, processed in a grasping forceps mechanism and in the control handle.

2. Design requirements

A number of design requirements need to be taken into account during the design process of the MonoFlex. These can be subdivided into (1) functional, (2) physical and (3) medical requirements. The functional requirements are describing the active controllable functions of the instrument. The physical requirements describe the geometry, material and production of the instrument. The medical requirements describe requirements that are clinically demandable. A subdivision into requirements and wishes has been made in order to make a distinction between high- and low-priority design requirements. During this research the focus is on the design of a grasping instrument with compliant joints, making the steerability, grasping force, and assembly requirements of Priority 1.

Table I: Design requirements subdivided into functional, physical and medical requirements.

	Description	Requirements	Wishes	Rationale	Priority
1. Functional	Steerability	1 DOF	> 1 DOF	The instrument should preferably be steerable in two directions as the DragonFlex, to obtain a higher functionality.	1
	Grasping force	> 2 N	> 10 N	The average force used to grasp light-weight flexible tissue lays below 10 N, but heavier tissues require a grasping force of about 10 – 20 N [30].	1
2. Physical	Diameter	8.0 mm		The choice is made to use this diameter because currently executed researches at TU Delft use the same diameter. In future, the working principles probably can be combined, making it highly useful to already use the same dimension. Due to confidentiality reasons, this cannot further be explained.	2
	Length	Between 24 - 45 cm		To approach the length of commonly used laparoscopic instruments, this range is chosen.	5
	Assembly	Main body non-assembly	Complete instrument non-assembly	In order to save assembly-time, the main body should be non-assembly. Only the control cables need to be assembled.	1
	Material	EnvisionTECVR NanoCure R5		The material is a relatively strong and hard polymer with a high flexibility, which made the DragonFlex tough and resistant. Because of these promising results, the choice is made to use the same material as used in the DragonFlex.	2
3. Medical	Ergonomics	Controlled like similar laparoscopic instruments	Haptic feedback during usage	The instrument should be safe, effective and easy to use.	4
	Safety	Torsion stiffness		This is important in order to obtain high reliability of the instruments during MIS. When, for example, the clinician rotates the instrument over its longitudinal axis, but the instrument is not torsion-stiff, the clinician does not know whether the instrument on the distal side is rotated or not.	3
		Bending stiffness			3
		Not allowing axial elongation			3

Table II: Properties of material R5 [12].

Property	Value
Tensile strength	31 – 39 MPa
Elongation at break	11 – 25 %
Elongation at yield	16 %
Modulus of elasticity	1.245 – 1.510 MPa
Flexural strength	40 – 45 MPa
Flexural modulus	1.190 – 1.383 MPa
Biocompatibility	No

The material properties of the material of choice, as described in Table I, are visible in Table II.

The length of the instrument and the ergonomics are considered not to be of high importance in this research. Of course these elements cannot be disregarded, but this research is of a different nature, being an exploration of a new working principle in the MIS field. The safety is explicitly of higher importance than the length and ergonomics of the instrument, but still subordinated to the functional requirements at this stage.

3. Concept Designs

3.1. Joints made by 3D printing.

3.1.1. Joint configurations. The design of different grasping forceps concepts that do not require assembly, mostly depends on the design of the joint(s) in the grasping mechanism rather than the graspers themselves. Nowadays, joints enabling rotational movements in one direction are used to move the two jaws of grasping forceps toward or from each other. When it comes to these joints, which are used to enable rotational motion in the tips of steerable instruments, a number of configurations are available, as suggested by Jelinek et al. [13]. As visible in Figure 3, a distinction could be made between rolling, sliding, rolling sliding, and bending joints.

During rolling, the two interfaces of a rolling joint rotate and translate with respect to each other, while sharing a moving point of contact. This contact area between the two joint halves is relatively small, which means that large friction between the surfaces is needed in order to transfer the motion. Gears and belts could be used additionally to transfer the motion and to prevent slipping of the surfaces. When it comes to slipping joints, the friction must be kept as low as possible because it could impede its rotation. A precise geometry of the joint halves is necessary to obtain a well working sliding joint. The rolling sliding joint, as indicated by its name, combines the rolling and sliding motion.

Where the rolling joints, sliding joints, and the rolling sliding joints make use of either a relatively high friction or a relatively low friction, bending joints on the other hand mostly depend on the dimensions of the flexural parts which enable the bending as well as on the material properties of the joints, such as the yield strength. The bending joint, or in other words compliant flexure joint, basically acts like a spring since it operates within the range of the material's elastic deformation and it is formed out of one piece. If the joint must be kept in a specific position, a continuous force is required. This is the case, because the joint will otherwise return to its neutral position, just like a spring. Overstretching the joint will induce plastic deformation, with a new neutral position as a result.

3.1.2. Non-assembly joints. To meet the design requirement of the instrument to be non-assembly, some joint configurations are excluded because not suitable. Among the rolling joints, the *rolling friction joint* and the *rolling toothed joint* need to be assembled, because both sides of the joints are printed separately (Fig. 3). Only the *rolling belted joint* would not require assembling when it is 3D-printed with the belt also 3D-printed, because both sides of the joint are already connected by means of the belts. When it comes to the sliding joints, both the *sliding curved joint* and the *sliding hinged joint*, in theory, could be printed at once, not requiring assembling. Support material can be printed within the space between the moving sides of the joint, creating one printable piece that does not require assembling. The *rolling sliding joint* is not suitable for non-assembly joints because both sides of the joints will be printed separately and require assembling. The *bending flexure joint* does not require assembling since it exists only of one single part.

To conclude, when it comes to non-assembly joints, it appears that only the rolling belted joint, the sliding curved joint, the sliding hinged joint, and the bending flexure joint are suitable.

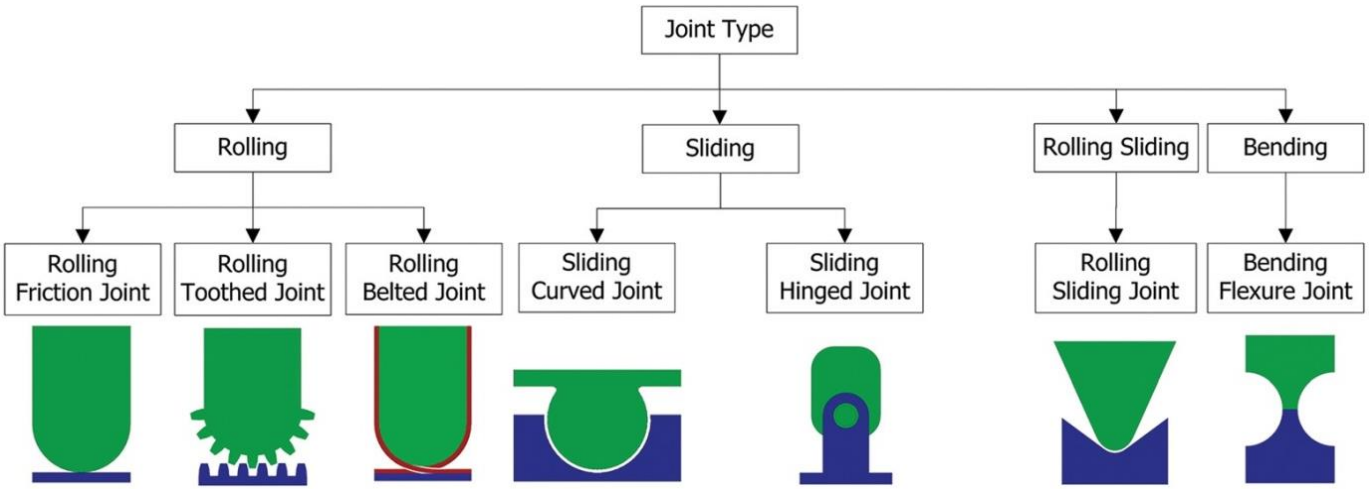

Figure 3: Classification of joints used for steerable instruments in minimally invasive surgery, retrieved from [13].

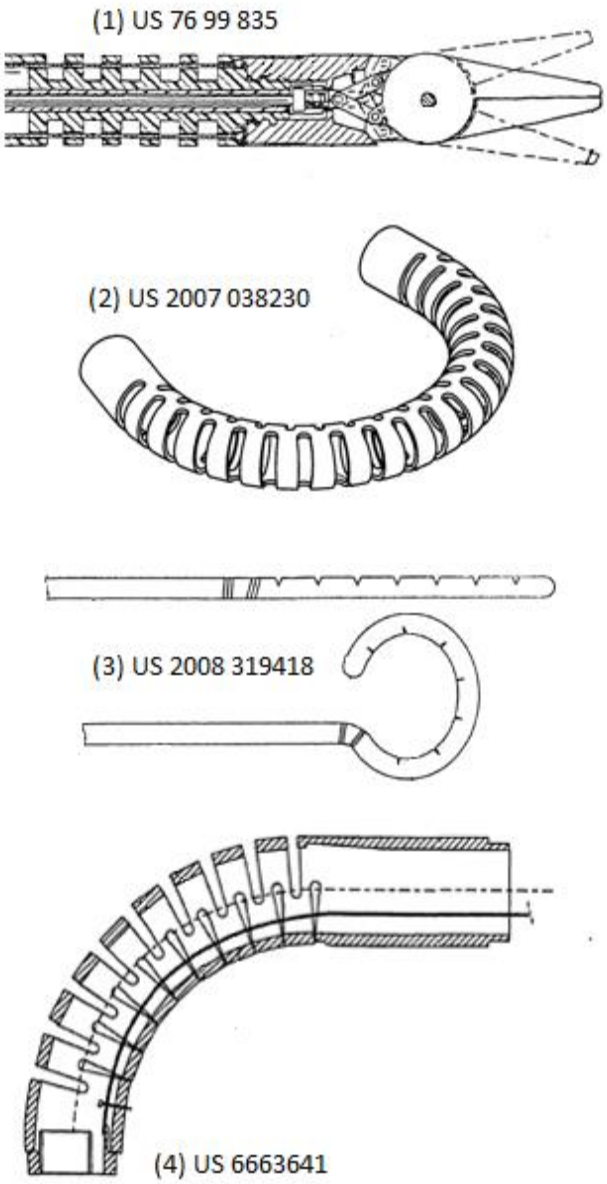

Figure 4: Overview of the bending flexure joints adopted from the patents (1) Lee et al. [18], (2) Stone et al. [26], (3) Chong [19], and Kovac and Wei [23].

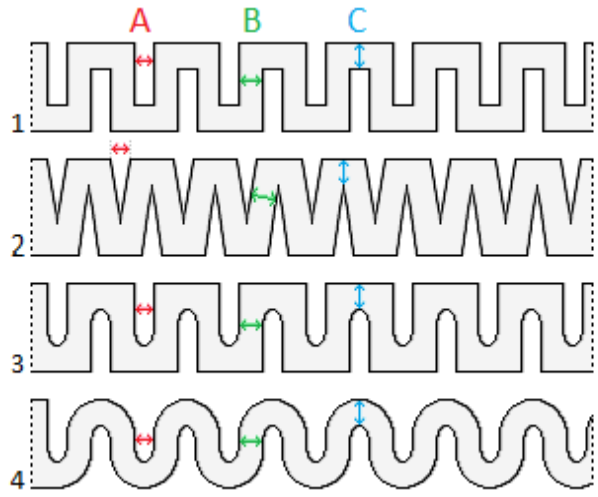

Figure 5: Rectangular, triangular, cylindrical, and wave geometries, with the gap width (A), material width (B), and material height (C) kept constant.

3.1.3. Joints printable with EnvisionTEC's Perfactory® 4 Mini XL. In theory, the four remaining joints can be 3D printed, however, it is not mentioned what type of additive manufacturing is used to print the joints. In this research, a photostereolithography printer is used with the material EnvisionTECVR NanoCure R5.

Non-assembly joints, existing out of multiple parts that move with respect to each other, are difficult to print due to the required space between the moving sides. As mentioned before, sliding joints need friction as low as possible, obtained by a precise geometry of the joint halves and smooth surfaces. However, the printing apparatus only allows printing separate parts when support material is added within the space between the parts. This means that the support material should be removed afterwards which is hardly possible without inducing imperfections on both joint sides, resulting in a decreased performance of the joint. This is the reason why the sliding curved joint and the sliding hinged joint cannot be used for this purpose. The rolling belted joint is also not suitable, because the belt needs to be attached very tightly to the joint sides, with the space between the belts and the joint sides so small that the printing apparatus will melt the belt and joint sides together during printing. The only joint configuration left is the bending flexure joint, made out of one single piece. Therefore, the principle of this joint configuration will be used for the design of the new surgical grasping forceps.

3.2. Grasping forceps mechanism.

The design of grasping forceps mechanisms depends on multiple factors including the choice of bending joint configuration, the joint(s) positioning, and the ways to control joints with steering cables or wires.

3.2.1. Bending joint geometry. Different bending flexure joints have been used and designed in the past for MIS instruments. These joints are compliant mechanisms with specific pieces of material removed, such that these can bend in at least one direction when one or multiple cables are pulled into a certain direction at the controller side (Fig. 4). Designs incorporating 1-DOF bending flexure joints are proposed in different patents [14-28].

In order to choose the best joint configuration for the the new surgical grasping forceps, simplified versions of the bending flexure joints found in literature are designed by using SolidWorks (2018). After this, the strengths of the different joint configurations are tested using the SimulationExpress tool, which is a FEM

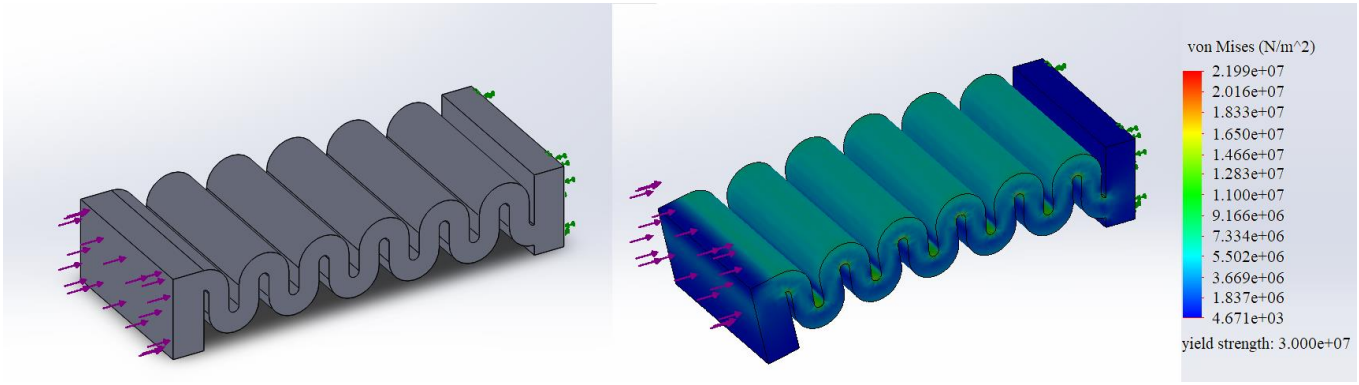

Figure 6: Simulation of the von Mises stress in a block with a wave cut out geometry. The block is constrained on the right side and an evenly distributed force of 10 N is applied on the left side.

software, available in SolidWorks. The material properties as mentioned in Table II are used, except for the Young's Modulus, which is measured during dog bone tests (Appendix A). The true Young's Modulus is found to be 1.048 GPa. All properties and belonging values are visible in Appendix B. In order to obtain the most reliable results with the SimulationExpress, it is necessary to use the right mesh size. In this case the smallest mesh size possible was 0.355 ± 0.0177 mm. An elaborated explanation of the influence of the mesh size can be found in Appendix C.

The basis for each joint design is a rectangular block with a cross section of 4.0 mm by 8.0 mm. The first design iteration shows four different cut out geometries, the so-called rectangular, triangular, cylindrical and wave geometries. In these geometries, the dimensions "gap width" (A), "material thickness in the horizontal direction" (B) and "material thickness in the vertical direction" (C) are kept the same among them, while the shapes of the cuts are different (Fig. 5). Drawings of the blocks before and after performing the simulation are visible in Appendix D. In order to simulate the maximum stress when compressing the blocks, evenly distributed forces are positioned on the designs. These forces are chosen to be 10 N (Ch. 2.), and placed on the left sides of the blocks, as visible in Figure 6. The results of the first simulation tests are summarized in Table III. Stress tensors in the material, which are not essentially uniaxial, that occurred after applying the force, can be mathematically written into a scalar, known as von Mises stress. This stress can be compared to the yield strength, which is the maximal stress allowed by the used material before yielding. As can be seen, the highest stress found in the triangular geometry is significantly lower than the highest stresses found in the rectangular, cylindrical and wave geometries (11.5 MPa vs. 15.7, 13.4 and 22.0 MPa respectively). The last value given in the table, the factor of safety, is a ratio between the yield strength of the material and the von Mises stress in the design, found with the simulation tool. When the factor of safety is below 1.0, this means the part will surely break when applying the force as simulated. For this MIS instrument design, is opted for a minimum factor of safety of 2.0, in order to be able to guarantee safety. Considering the simulation results, the triangular geometry is the most promising geometry, because of the low maximum stress and the high factor of safety Normally, sharp edges or cuts are not recommended to be used, since they can act like cracks in the material, which propagate catastrophically [36]. For cracks or grooves with a crack tip radius of nearly zero, the stress would tend to infinity. In Appendix C is explained why these stress concentrations sometimes cannot be measured, depending on the mesh size in the FEM software. However, the research is continued using this geometry, since the smallest mesh size possible is used, and because it is interesting to compare the simulation results with the actual outcome and the known theory.

Table III: Stress and factor of safety found in cylindrical, rectangular, triangular, and wave bending joint geometries, when applying a force of 10N imitating the control cables.

Geometry in block	Von Mises stress [MPa]	Factor of Safety [-]
Rectangular	15.7	1.9
Triangular	11.5	2.6
Cylindrical	13.4	2.2
Wave	22.0	1.4

The triangular geometry is implemented in a grasping forceps design (Fig. 7). To be able to simulate what will happen to the geometries when a cable pulls on the distal end of the joint to open it, forces acting like control cables are positioned on the designs. These forces are again chosen to be 10 N, and placed in cuts which imitate the cable fixation points on either the top or the bottom side of the jaws of the grasping

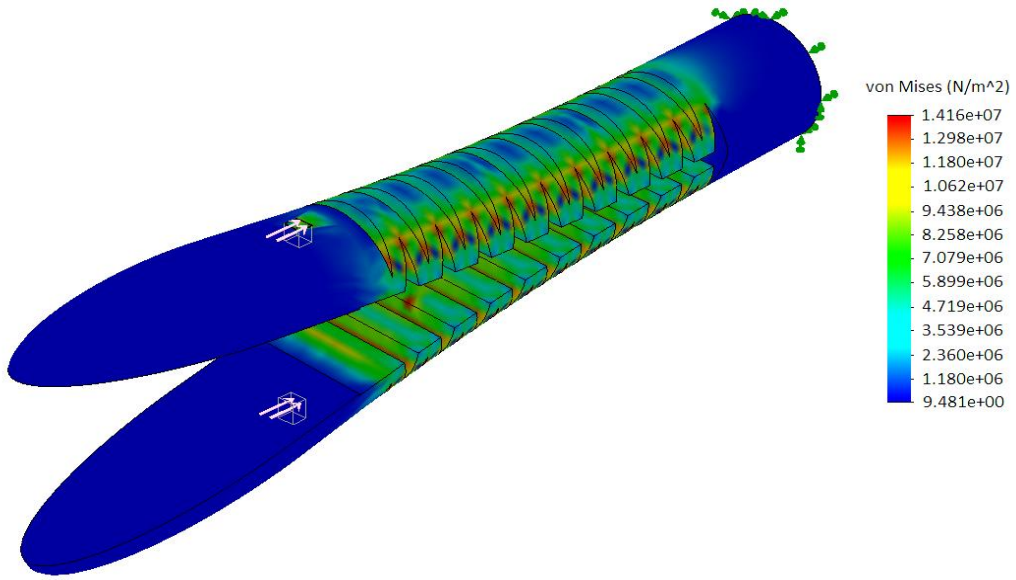

Figure 7: Simulation of the von Mises stress in grasping forceps with triangular geometry. The pink arrows point out the location and direction of the forces which imitate the forces applied by the control cables.

mechanism, as visible in Figure 7. These locations are chosen to be the cable fixation points, in order to maximize the moment arms. The found von Mises stress in this case is 14.4 MPa, which is a bit higher than in the "block test" case. This is possibly due to the halve-circular cross-section of the grasping forceps jaws, which are less strong than the block with the rectangular cross-section, and due to the change of location of the applied force. The aim is to design a grasping mechanism which can open up to 90°, which means the displacement at the distal side of the joint should be 6.0 mm. In this case this displacement from the original position was found to be 5.0mm and therefore not yet as required. By tuning the dimensions A, B and, C (Fig. 5), the properties of the joint can be adjusted until the mechanism reaches a strength and flexibility which are needed to meet the requirements and which show the optimal response to the forces applied by control cables of wires.

While simulation tools such as in SolidWorks can give an idea about how instruments or mechanism should work in real life, in reality, it will be different after all. Therefore, conflicting with the simulation tool in SolidWorks, another bending joint geometry is proposed as well. This joint is based on the leaf-spring principle and basically consists out of one thin horizontal layer of bending material, with some extra material only used to guide the control cables, see Figure 8. This geometry also could be considered as a rectangular or cylindrical geometry with the gap width (dimension A, Fig. 5) the same length as the complete joint. According to the simulation tool, this bending joint geometry is not strong enough to withstand the moment obtained by the control cables, and the expectation is that it will break. However, since the usefulness of leaf-springs made of different materials is widely known, and since the properties of the used material in this case are promising as well, the choice is made to elaborate this joint geometry further as well.

3.2.2. Straight vs. pre-bent joint. The bending flexure joint is controlled by cables which need to be integrated into the joint. Depending on the joint configuration, or the way in which the joint is printed, the number of cables can differ. A joint that is printed straight can be in three different states, namely in the closed state (Fig. 9(a)), in the neutral state (Fig. 9(b)), or in the opened state (Fig. 9(c)). The neutral state is the state where the grasping forceps are not actively opened or closed. The whole instrument is straight, but

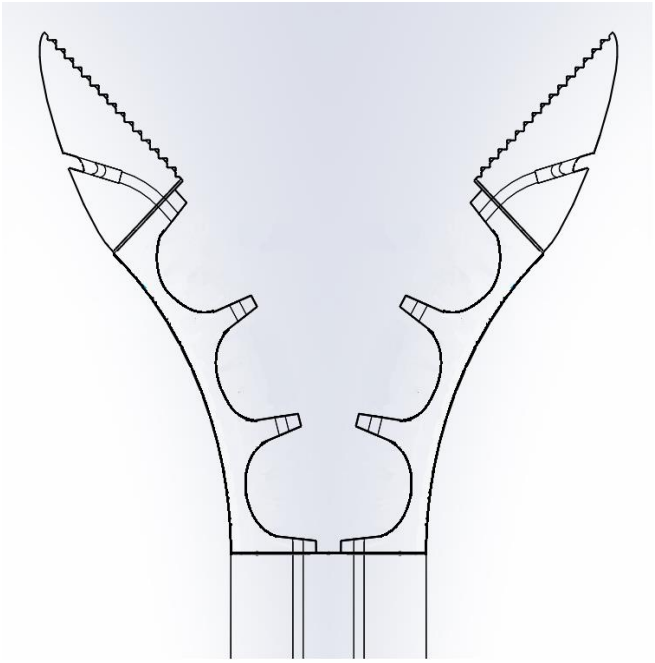

Figure 8: Alternative joint geometry, consisting out of a thin bending layer with small material attachments to guide the control cables.

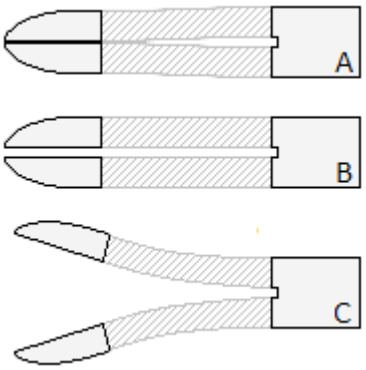

Figure 9: The three states of a joint which is printed straight. (a) Closed state, (b) neutral state, (c) opened state.

there is space between the two grasping jaws. The closed state is the state where the grasper forceps are completely closed and there is no space between the grasping jaws left. The opened state is the state where the grasping jaws are opened actively, up to a total angle of 90º. When the grasping jaws are released after opening or closing, in an optimal case the grasping jaws will return to the neutral state due to the elasticity of the material. However, plastic deformation is a well-known problem occurring in plastics that are bent alternately in different directions, especially when the geometry of the bent area is thin. This means that the neutral position of the straight printed joint could change over time. To open the grasping forceps, at least one cable on the top side of the jaw is necessary, and to close the grasping forceps, another cable on the bottom side of the jaw is necessary. However, in this case, it is challenging to fixate the cables on the forceps side of the instrument. This problem can be prevented by creating a loop of each cable on the forceps side of the instrument, making them go back and forward through the whole instrument. So in this case, on the control handle side, two cables must be pulled to open one of the jaws (four cables to open both) and two cables have to be pulled to close one of the jaws (four cables to close both). In total there will be eight cables on the control handle side of the instrument when using a straight printed bending flexure joint (Fig. 10).

An alternative joint configuration to the straight printed version is the pre-bent joint configuration. In this configuration, as the name says, the jaws are pre-bent outwards. The pre-bent joint can, in contrast to the straight printed joint, be in two different states. The first state is the neutral state, which simultaneously is the opened state. The second state is the state where the grasping forceps actively are closed by pulling the cables which in this case only are connected on the bottom side of the jaws. When after closing the grasping forceps, the cables are released, the jaws will go back to their neutral state due to the elasticity of the material. This means that the grasping forceps open passively, without any additional force. However, the same problem arises as mentioned in the straight printed configuration case. Plastic deformation occurs in plastics which are bent alternately in different directions, resulting in a shift of the neutral state. With the pre-bent joint configuration, this implies that the grasping forceps will open less over time due to the absence of active opening control. This makes the instrument less durable than the straight printed joint

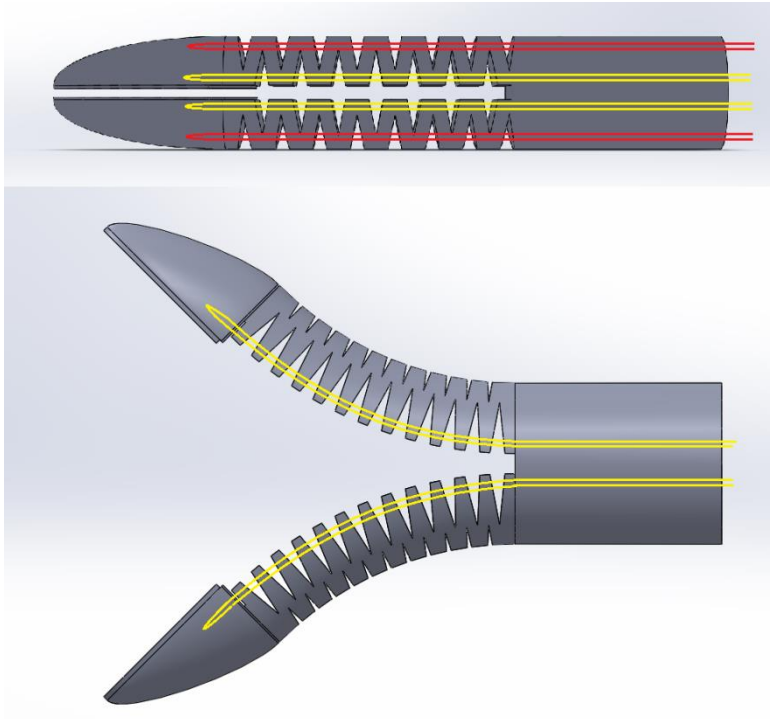

Figure 10: Straight and pre-bent grasping forceps showing yellow cables to close the grasping forceps, and red cables to open the grasping forceps actively in case the mechanism does not open passively due to elasticity.

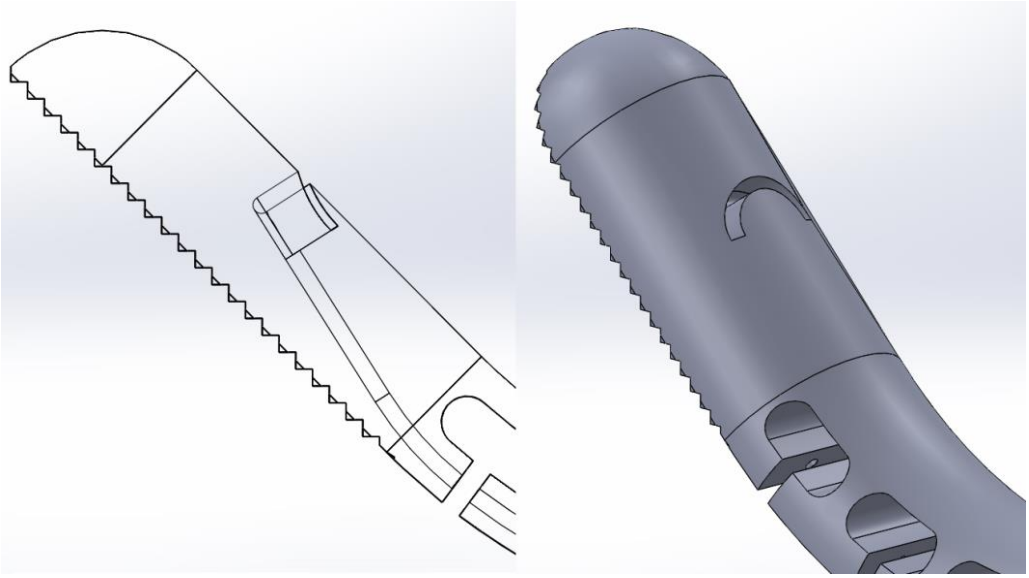

Figure 11: Cross section and 3D view of grasping forceps tip with control cable slot and groove on top of the tip leading to the slot.

configuration, but because of the intended disposable nature of the instrument, this is not a problem. An advantage of the pre-bent joint configuration over the straight configuration is the lower amount of cables required to control the grasping forceps, making the design simpler (Fig. 10).

3.2.3.Control cable vs. control wire. Depending on the choice of cable or wire, the design of the grasping forceps mechanism should be adjusted. The main difference in the design does not rely on the diameter of the cable or wire, but more on the behaviour of cables or wires. A cable basically exists out of multiple smaller tangled wires, making it flexible and thus easy to bend. This is an advantage in inserting the cable into a slot which is not exactly straight. Instead, a wire with the same diameter will be much stiffer, making harder the insertion in curved slots. However, this stiffness also has an advantage, because where the cable can only be used to control the grasping forceps by pulling and thus closing or opening it, the wire can be used both to close and open the grasping forceps by pulling and pushing.

When a cable is used to open or close the grasping forceps, it will go back and forward through the whole instrument creating a loop on the forceps side of the instrument. In this case, it is enough for the slot to end on the top side of the grasping forceps jaw tips, resulting in a cable loop on the outside of the instrument. When a wire is used instead, the design of the slot needs some adjustments such that the wire can actually be pushed, without leaving the slot. This can be realised by designing the slot deeper in the jaw tips, such that there is the material of the jaw tip itself to push against (Fig. 11). Perpendicular to the slot, a groove is designed, such that the outside of the jaw tip and the slot are connected. The wire can now be inserted in the slot via the groove, but once it is inserted, it will never come out again by itself.

3.3. Control handle.

On the other side of the instrument, opposite to the grasping forceps, the control handle is placed. The aim

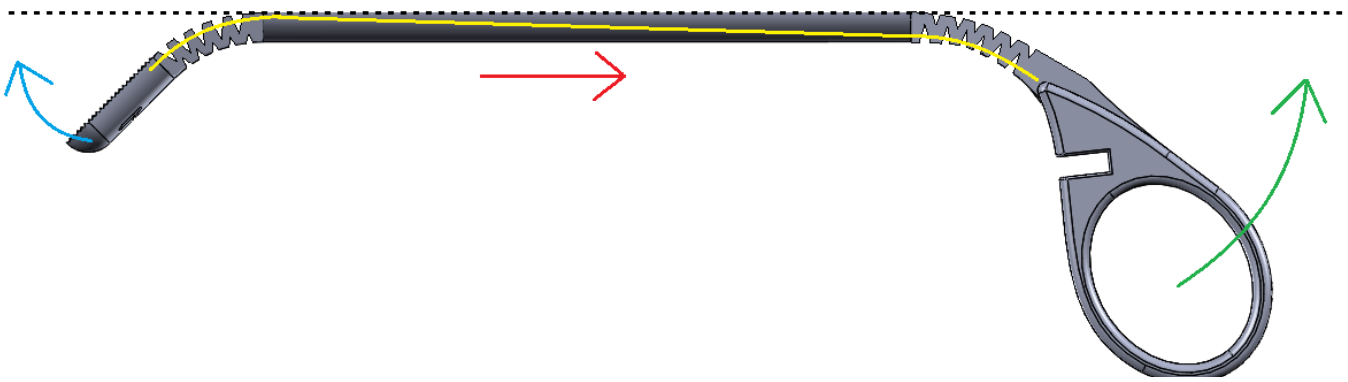

Figure 12: Bending joint configuration placed upside-down on control handle side. Closing the control handle (green arrow) results in a pulling force (red arrow) on the yellow cable, with makes the grasping forceps close (blue arrow).

is to make the control handle out of one part as well, similar to the grasping forceps. Previously, the control handle for the DragonFlex is ergonomically optimized during a process of designing and testing. That is the reason why the same 3D-drawings are used for the the new grasping forceps. However, the parts designed for the DragonFlex do not have compliant joints but require assembly after printing. This problem can be fixed by putting the parts together and using the same complaint joint geometry as used for the grasping forceps jaws. The choice of bending joint geometry is based on the printing iterations, which will show the best geometry after testing.

The joints in the control handle must be reversed compared to the bending joint used in the grasping forceps (Fig. 12). When the control handle is closed, or in other words, the jaws of the control handle are bent inwards, the grasping forceps jaws have to close as well. The control cables on the grasping forceps side are guided through the inner sides of the bending joints. This means that when the cables are pulled in the direction of the control handle, the grasping forceps are closed due to the shortening of the inner side of the bending joint relative to the outer side of the bending joint. The joints bend inwards and close the grasping forceps. On the control handle side, the opposite should occurs. When the control handle is closed, the side where the control cable is guided through has to elongate. This is the case when the cable is guided through the outer side of the bending joint. This side elongates relative to the inner side of the joint when closed.

4. Printing iterations

4.1. Grasping mechanism printing iterations.

As mentioned in Chapter 3, an iterative design process was used to find the most suitable grasping mechanism design, which was also durable. The process in this section describes the different printing iteration rounds performed. Each iteration describes the designs that are printed with belonging dimensions and the results found after testing and analyzing the printed parts. A comparison between the drawings and the printed parts is made as well. In Appendix E, the possible consequences of small changes in the design are described with both, stress and displacement simulations.

*4.1.1. Iteration I: Simulation-based design***.** The first printing iteration includes designs developed using the SimulationExpress tool in SolidWorks. During an iterative process the optimal bending joint geometry, according to the tool, was found. The triangular geometry was considered to be the best bending joint geometry and therefore used during the remaining optimization process. This geometry with belonging dimensions is visible in Figure 13(a). Figure 13(b) shows a photo of this specific design after printing.

Some geometrical and functional differences compared to the 3D digital design clearly occur. The grooves which are the basis for the bending mechanism of the bending joint were drawn on the top

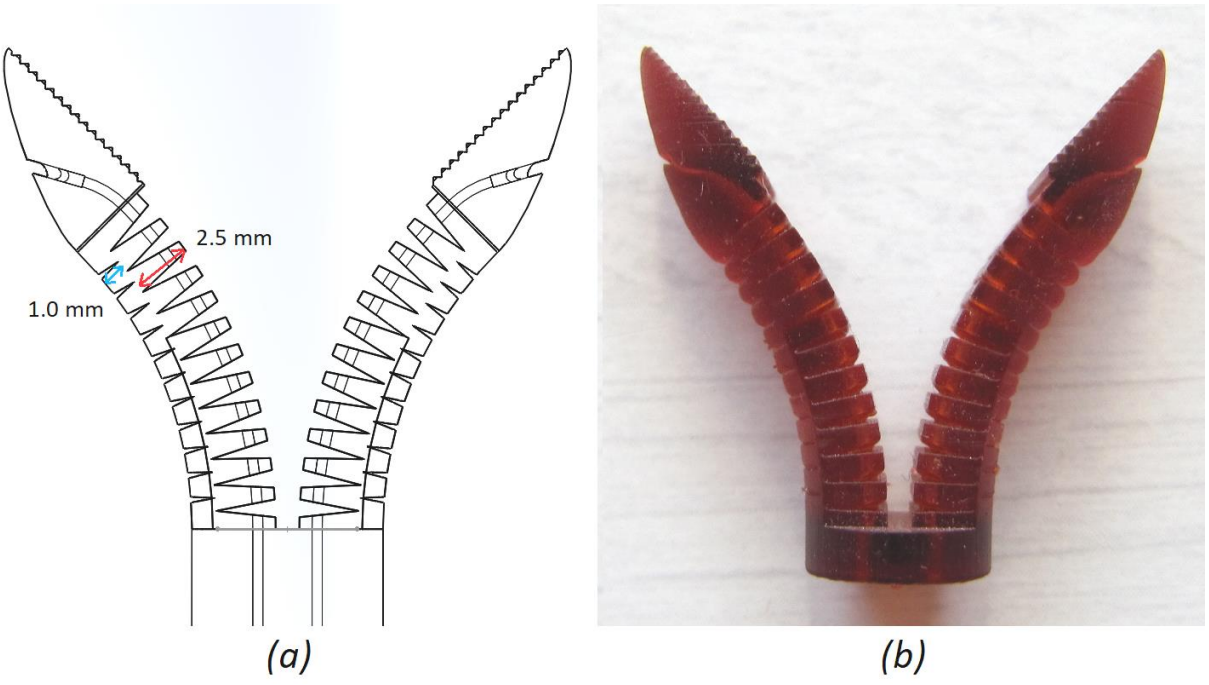

Figure 13: Part made in iteration round I. (a) Front-view of digital drawing, (b) front-view of 3D-printed part.

and bottom side of both jaws. After printing, these grooves are silted up, resulting in a lower functionality. The grasping forceps is stiff and cannot be closed completely without breaking. The grooves on the outside of the jaws are drawn with a length of 1.0 mm, but after printing, only grooves with length 0.1-0.4 mm can be measured. The grooves on the inside of the jaws are drawn with a length of 2.5 mm, but after printing the grooves are only 0.5-1.2 mm long. Thus, The printing accuracy of the grooves, in this case, is approximately 10-48%. Uncured resin which stays in the grooves due to cohesion forces, can cure after all when exposed to UV-light, by means of UV-lasers or in daylight [33]. Since the grooves are very tiny towards the middle of the joints, resin can easily stick there and silt up the grooves. The cable slots, as visible in Figure 13(a), are also visible in 3D in Appendix F.

To obtain printed parts that have similar (groove-) dimensions as the drawing, the grooves in the drawing must be adjusted such that geometrical errors found in the parts printed during the first iteration will be compensated during the second iteration.

4.1.2. Iteration II: Simulation-based design (adjusted 1.0). The second printing iteration is based on the same drawing optimized by the SimulationExpress tool in SolidWorks, but in this case, the design is adjusted to compensate for the errors found after printing. The drawing with belonging groove-dimensions is visible in Figure 14(a). As can be seen, the dimensions of the grooves are way thinner than these dimensions after the optimization process and iteration I. The idea is that when the grooves are drawn larger, they will approach the dimensions of the optimized drawing after printing, taking into account the silting up of the grooves during printing. After printing, the parts looked like the photo of Figure 14(b). The first observation showed an improvement in flexibility of the bending joint. Now, the joint can easily close, making both jaws touching each other. However, when a close look is given to the bending joint, it can be seen that neither the grooves nor the material between different grooves are equal in dimensions or equally distributed over the whole joint. The material between the grooves on the proximal side of the bending joint is much thicker than the material between the grooves on the distal side of the bending joint. This is not due to the distribution of the grooves compared to each other, but rather on a change in dimension of grooves over the joint. The lengths of grooves on the proximal side of the joint are smaller than the lengths of grooves on the distal side (0.5 vs. 1.5 mm (outside) and 2.0 vs. 2.5 mm (inside)). The shapes of the grooves are different than in the digital drawings as well. The shapes should be triangular, but instead, on the distal side of the bending joint, they are more parabolic-like. Further analysis of the printed parts showed that the top side of the bending joints is not in line with the top sides of the tips of the grasping forceps, which should be the case. The height of the bending joint in total is drawn to be 3.5 mm, however, the printed part shows a height of 3.0 mm at the distal end of the joint, just proximal to the tips of the grasping forceps.

All the previously mentioned differences contribute to the problem of the differences in material thickness alongside the bending joint. When the material is thinner on a specific location on the bending joint, this automatically makes this location more flexible, but also more fragile. This problem of location-based fragility is also encountered after manually testing the parts which were printed during the second iteration round. When the jaws of several similar grasping

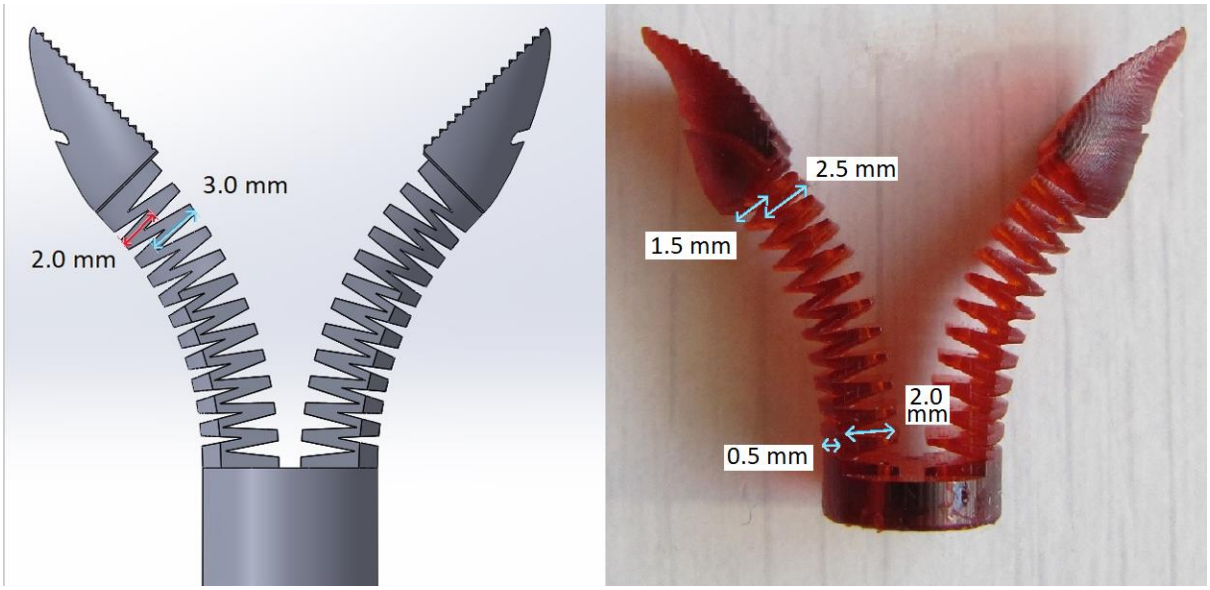

Figure 14: Part made in iteration round II. (a) Front-view of digital drawing, (b) front-view of 3D-printed part.

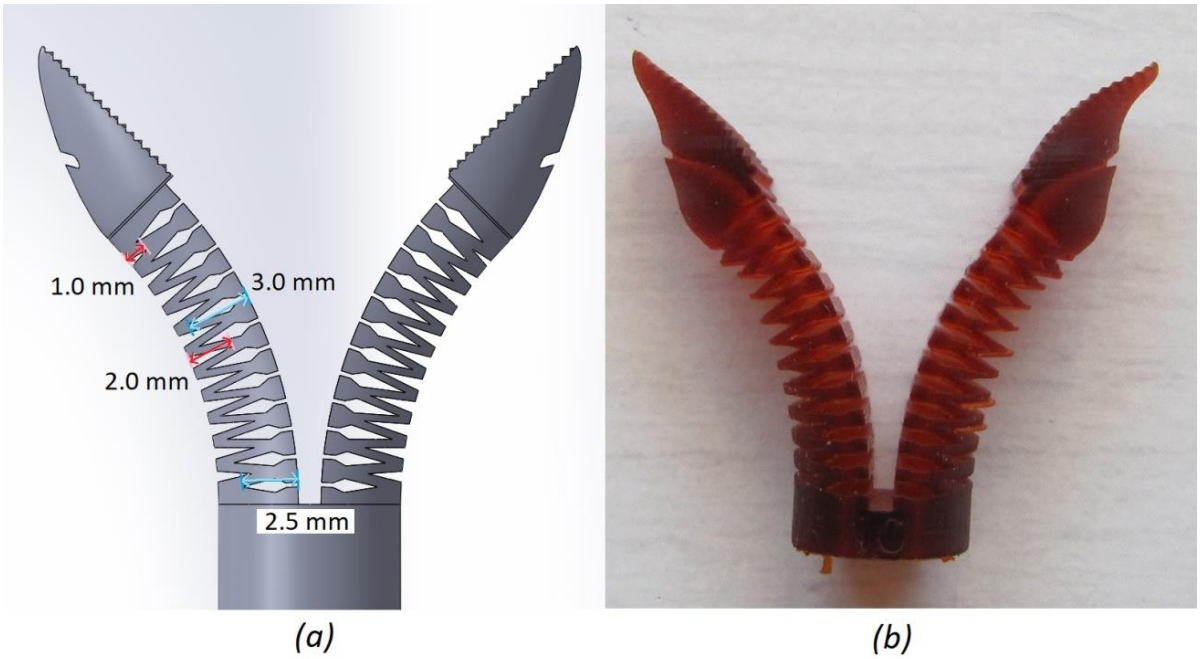

Figure 15: Part made in iteration round III. (a) Front-view of digital drawing with varying groove-dimensions (inside grooves: 2.5-3.0 mm, outside grooves: 1.0-2.0 mm) , (b) front-view of 3D-printed part.

forceps were opened and closed alternately, the bending joints did break in most cases, and in all these cases just behind the jaws, on the previously determined fragile spot.

Another observation that shows a difference between the intended geometry and actual geometry after printing is the jaw tip, which is warped while the inside should be straight (not considering the grasping teeth). The extent to which this problem occurs, differs from case to case, on a random base. Warping of thin structures is investigated more often in literature and is caused by temperature differences between the different printed layers [34]. Differences in temperature causes differences in material properties, which again causes internal stresses, making the jaw tips warp.

4.1.3. Iteration III: Simulation-based design (adjusted 2.0). In the third iteration round, an attempt is made to solve the errors found on the parts which were printed in iteration II. The main problem that occurred was the change in groove sizes alongside the bending joint, resulting in extreme thin structure-zones, creating high fragility. For this reason, the designs are adjusted in such a way, that the heights should be similar for all grooves after printing. In iteration II, the more distal the grooves were located, the larger they became. Therefore, the more distally located grooves are made smaller in iteration III. Also, the most proximally located grooves where fragile and likely to break, so therefore also these grooves are made smaller in iteration III. The lengths of the grooves on the outside of the jaws vary from 1.0 to 2.0 mm. The grooves on the inside of the jaws have a length between 2.5 and 3.0 mm. The drawing with belonging groove-dimensions is shown in Figure 15(a). Another difference of the drawing in iteration III, compared to the drawing in iteration II, is the addition of material on the inside of the jaws, which prevents the bending joint geometry to bend too much at any specific spot.

Figure 15(b) shows one of the parts being printed. As seen in previous printing iterations, some areas of the bending joint geometry are thicker than drawn in the digital drawing. However, it is remarkable that there are also areas in the middle of the bending joint which are thinner than in the digital drawing, making the design very fragile. During manual testing the parts, several parts broke on the same spot in the middle of the bending joint. The functionality of the parts is improved compared to the previous iteration round because of the added material on the inside of the jaw. However, the parts still are very likely to break after alternately opening and closing the jaws. Due to the medical purpose of the grasping mechanism, which should be used inside a human body, this lack of sustainability makes the design unreliable. Therefore, further analysis of this simulation-based bending joint geometry was discontinued. An alternative design was analysed instead, as described in the next section.

4.1.4. Iteration IV: Alternative design. The grasping forceps with the alternative bending joint geometry consists out of one thin layer of bending material, with

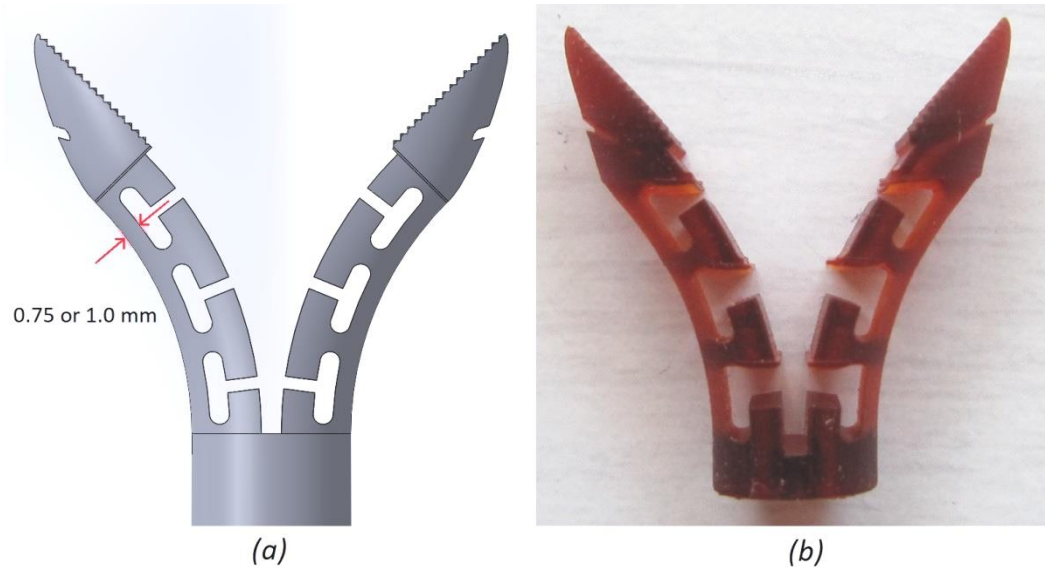

Figure 16: Part made in iteration round IV. (a) Front-view of digital drawing of thin-layer bending joint geometry, (b) front-view of 3D-printed part.

some extra material attached, only used to guide the control cables. Figure 16(a) shows the alternative design. As can be seen, the bending layer is placed on the outside of the joint, and this geometry is pre-bent as well, just as the triangular bending joint geometry described above. The thickness of the bending layer is 1.0 mm. During printing iteration IV, this design, and also a similar design but with bending layer thickness 0.75 mm, are printed. Immediately after the first manual tests, the functionality of these alternative designed joints seems highly promising. The flexibility is equally divided alongside the joints and no specific fragile spots can be detected. Alternately opening and closing the jaws, does not make the joints break, and no visible cracks appear. When compared, the design with a bending layer thickness of 1.0 mm, the strength-flexibility ratio seems perfect, while the design with the bending layer 0.75 mm thick, is slightly too flexible and thereby less durable and functional.

Even if these first prototypes show promising results, there are also obvious errors in the parts, compared to the digital drawings. The first error to mention is similar as in iteration II and III.

The jaw tips are warped outwards, while the inside of the tips should be straight. This happens on a random base. Another error in the printed parts is visible on the extra material used to guide the control cables. These attachments have a T-shape in the digital drawing (Fig. 16(a)), however, one part of this T-shape is not printed properly, as visible in Figure 16(b). Besides guiding the control cables, these T-shape attachments are also designed this way to control the way in which the joint bends when a force is applied by using the control cables. When different T-shape

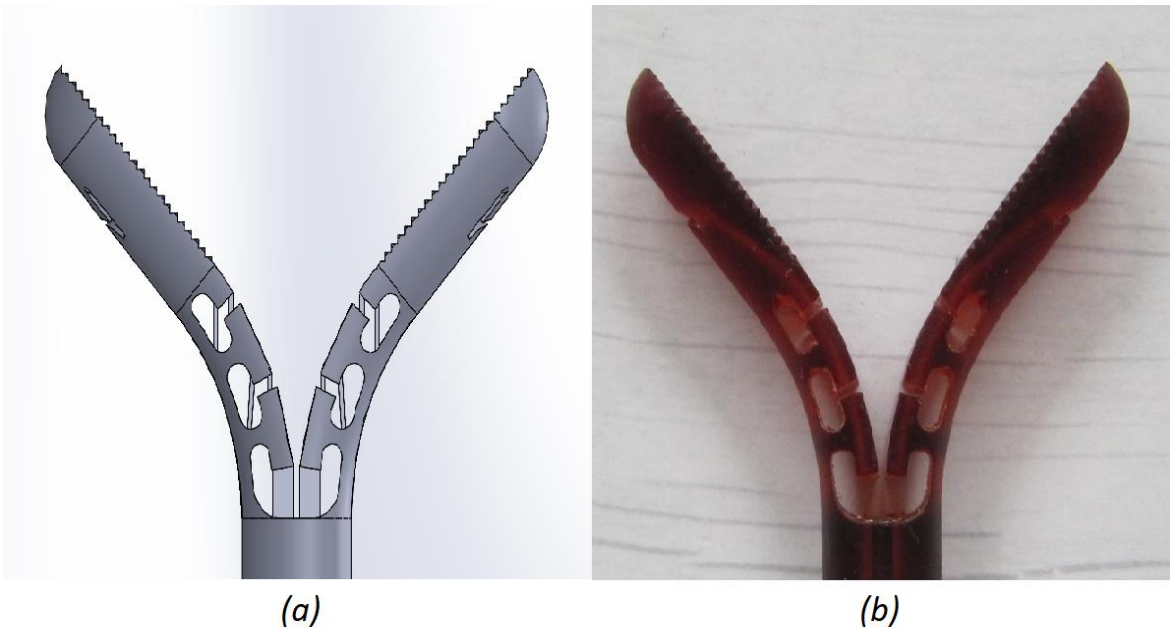

Figure 17: Part made in iteration round V. (a) Front-view of digital drawing of thin-layer bending joint geometry, including support material, (b) front-view of 3D-printed part after removing support material.

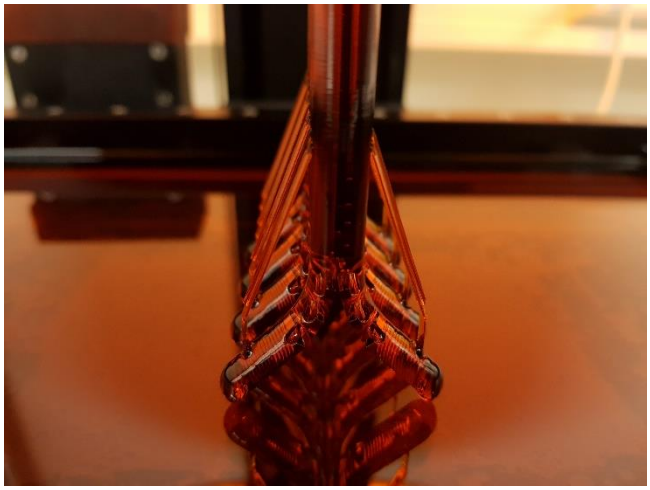

Figure 18: Parts during VAT photo-polymerisation printing process. Photo made by P. Breedveld, 2019.

Figure 19: Control handle as used in the DragonFlex, existing out of multiple parts, connected via gear wheels. Adapted from [10].

attachments touch, this blocks further bending of the thin layer of bending material between these attachments. In this way, the stress in the joint can be divided equally alongside the joint, and the joint does not bend too far on one location while the joint does not bend at all on other locations. However, as mentioned before, these T-shapes are not printed properly, losing the function of preventing overly bending. Iteration V focuses on the improvement of these two geometry printing errors.

4.1.5. Iteration V: Optimized alternative design. Two different errors are found in the parts printed during iteration IV: first, the wrapped tip and second the improperly printed T-shape attachments. The reason why the tip is wrapped is, as described earlier, probably due to internal stresses in the material that develop during the VAT photopolymerisation due to temperature differences between the different printing layers. These stresses can wrap the thin design of the grasping forceps jaw tips. One way to solve this problem is simply to make the design larger, such that the internal stresses will not predominate and the tip will not wrap. The tip is redesigned and made twice as long as the tip in the designs of the other iterations. It is also less sharp and more rounded, such that there are no thin locations which could possibly wrap, see Figure 17(a).

The problem of the improperly printed T-shape attachments is caused by a lack of support. When the design is printed vertically as visible in Figure 18, the upper parts of the T-shape attachments, so to speak, float in the air. Since air cannot provide any structural support, this results in the improperly printed parts. To solve this problem, in iteration V, extra support material is added right above the missing parts of the T-shape attachments in iteration IV. After printing, the support material is removed and the result is improved drastically (Fig. 17(b)). The slot and groove as designed in the digital drawing, are suitable for the use of control wires instead of control cables. Manual tests prove that the functionality of the grasping forceps tip is as desired and expected. A last manual test showed that a control wire length difference (shortening of wire on grasping forceps side) of approximately 2 mm is required to be able to fully close the grasping forceps. When this length difference can be obtained by elongating the wire on the control handle side, the complete instrument should be able to function.

4.2. Control handle printing iterations.

4.2.1. Iteration I: Adjusted DragonFlex control handle. The control handle as used for the DragonFlex, exists out of multiple parts which have to be assembled and are kept together by the tension of inserted control cables. The objective of this design project is to minimize the assembly time by making a non-assembly printing part, which also includes the control handle. This can be done by inserting the same complaint joint structure used for the grasping mechanism, as described in Section 3.3. The original DragonFlex control handle design includes two control handle halves, both with gears that exactly fit on the connection parts leading to the grasping jaws, as shown on Figure 19. In the new design the gears are replaced by compliant joints and attached together, making one fully assembled control handle instead of two control handle halves which need assembly. The adjusted control handle is printed and manually tested (Fig. 20). Close-up images of the digital drawings are visible in Appendix G.

Three major observations can be mentioned. First, the design looks promising, based on the way it bends when pushed together. The joint functions and should be able to pull the control wire when the control handle

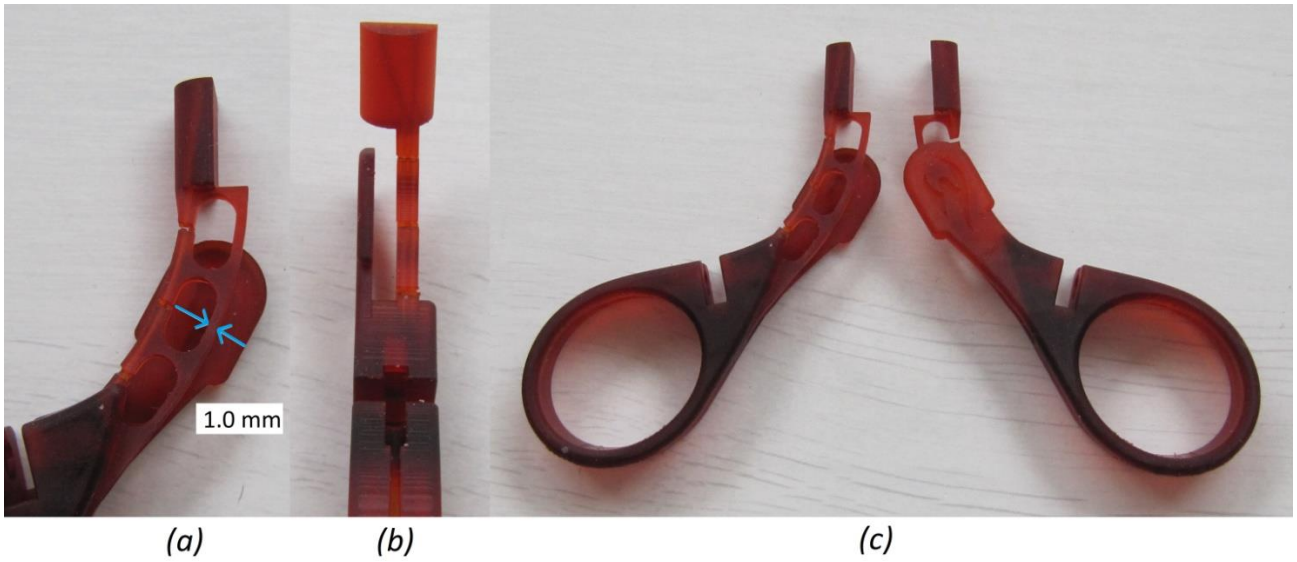

Figure 20: Control handle halves. (a) Front-view of compliant joint structure, (b) side-view of control handle halve, (c) two whole control handle halves.

is closed and push the wire when opened. Second, the joint is too thin and too flexible. The control handle cannot stand its own weight without bending. When the control handle is kept vertical, with one half above the other, both the upper and the lower halve bend downwards. This problem can be solved by simply thickening the bending layer of the compliant joints. This will strengthen the joint, and making it more stable. Third, the control wire cannot be inserted through the specially designed slot. This is due to an internal curve of the slot which is too sharp for the stiff wire. In iteration II for the control handle, is tried to overcome these problems.

4.2.2. Iteration II: Optimized control handle. As mentioned previously, in iteration round I, the control handle bending joint is too thin and flexible. This problem can be solved by thickening the bending layer. The thickness is now set to 1.5 mm, instead of 1.0 mm. Other major changes to the drawing are, first, the control handle halves which are put together, forming one solid part, and second, the displacement of the control wire slots. The part is printed and the result is visible in Figure 21.

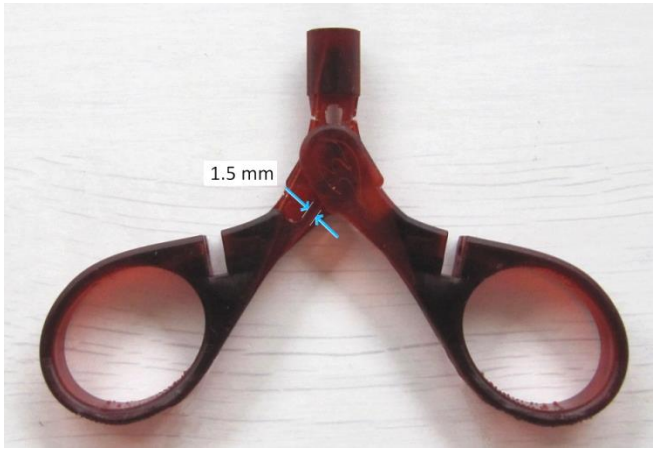

Figure 21: Control handle from iteration II, with 1.5 mm bending layer.

The first manual testing showed improved stability of the complete control handle. This can both be due to the thickened bending layer, as well as to the fact that this part is printed as one solid part instead of two separate parts. The thickened layer on itself is also improved and stiffer than during the first printing iteration. When the handle is closed and then released, both sides of the control handle move back to the neutral position, which is the position or state in which the part is printed, thus fully opened. As mentioned in Section 3.2.2, the neutral state of the compliant joints in the control handle can shift over time due to plastic deformation as a result of alternately opening and closing the part. However, since the control handle will be used and controlled manually anyway, this is not a problem for the control handle. Moreover, the fact that both sides of the control handle easily move back to the neutral position emphasizes the improvement of the stability. Also, when the control handle is kept vertical, just as in iteration round I, both sides stay in place instead of bending downwards.

Furthermore, the slots for the control wires are slightly displaced, compared to iteration I. This solves the problem of the wires, which could not be inserted in the slots, and the wires can be inserted in and passed through the slots without any difficulty.

A manual test is performed to test the working principle of the bending joint on the control handle when controlled by the control wire. While the cables are not fixated yet, an elongation of the wire going through the control handle can be measured when closed. The length difference of the wire going through the control handle when fully opened and fully closed is approximately 3 mm, which means that the control

Figure 22: Separate grasping forceps part and control handle part attached and connected by a (non-fixated) control wire. Left: instrument opened, right: instrument closed.

wire difference of 2 mm which is required to be able to fully open the grasping forceps, can be reached (see Section 4.1.5.). Therefore, when it comes to this issue, the combination of grasping forceps and control handle should be functional.

4.3. The complete instrument

Now that grasping mechanism and the control handle both are optimized and show promising results, they have to be put together to see whether the complete instrument had the desired outcome, with a proven working principle. This section is divided describes the prototype with two separated printed grasping forceps part and control handle part, put together, and the final one-part 3D-printed instrument: MonoFlex.

4.3.1. Combination of grasping mechanism and control handle. The final grasping forceps mechanism found in Section 4.1.5. and the control handle optimized in Section 4.2.2. are, with some small adjustments, used together. In order to be able to use the separate parts combined, the designs are adjusted such that these can be slid over each other, while tensed wires keep the parts together. Figure 22(a) and 22(b) show the parts when combined. During the manual tests performed at this stage, both sides of two control wires are inserted each on one jaw of the grasping forceps, whereafter they are guided through the control handle and come out at the other side of the control handle. The wires are tightened until a loop forms at the grasping forceps side and this loop is placed in the specially designed control wire groove. Once the wire is placed in this groove, it will never come out without using additional tools. The wires are not fixated yet on the control handle during this first manual test of the parts in combined use, due to missing parts for the fixation.

When both the grasping mechanism and the control handle are opened as much as possible (Fig. 23(a)), closing the control handle results in a closing of the grasping forceps mechanism until the jaws touch each other (Fig. 23(b)). Although the wires are not fixated yet, the friction between the wires and the printed parts is high enough to allow this movement. On the other hand, the result is also that no force can be applied with the grasping forceps.

It is expected that when the control handle is opened, the grasping forceps will also open due to the wire, which pushes against the tip of the grasping forceps, at the spot where the control wires makes a loop. However, the wire is still not fixated yet, which

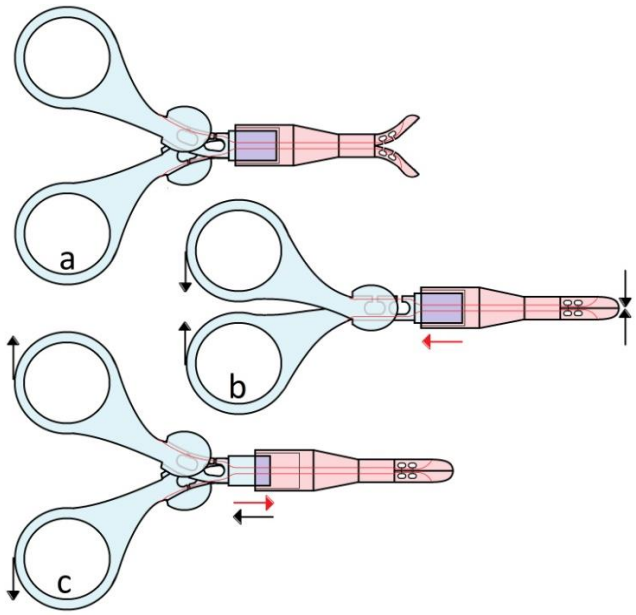

Figure 23: Combined grasping forceps and control handle. (a) Fully opened, (b) control handle closed → pulling control wire (red arrow) → closing grasping forceps, (c) control handle opened → pushing control wire (red arrow) → pushing control handle out of grasping forceps part (black arrow)

also has an influence on this manual test. When the control handle is opened, the grasping forceps does not open immediately. The wire on the control handle side shortens when opened, resulting in an elongation of the wire on the grasping forceps side, if it works as expected. However, since the parts are slid over each other, but not attached or glued yet, there is play between the parts, allowing movement of one part relative to the other part. So if the wire between the two parts is elongated due to a shortening of the wire on the control handle side, the wire basically pushes the two parts apart, instead of opening the grasping forceps, see Figure 23(c). When the parts are kept together by hand, this problem does not occur and the grasping forceps open up to 90°. The conclusion of this manual test is that the combination of the control handle and grasping forceps mechanism shows promising results. The next step is to print these parts together, attached, forming one single part.

4.3.2. MonoFlex unsteerable. As found in the previous section, the combination of the grasping forceps and the control handle show promising results. In this section, these two separate parts are printed for the first time as one part, approaching the goal of the research project. The parts printed in this iteration round are basically the final parts printed in Sections 4.1. and 4.2. with a longer axis between the two parts, all connected to each other. Figure 24(a) shows the printed part.

The control wires are guided through the whole instrument and fixated on the control handle side of the instrument. The fixation is obtained by a mechanism using a screw bolt in which the wire is fixated and a nut which enables manually changing the tension on the wire (Fig. 24(b) and 24(c)). Inside the screw bolt, a hole is drilled, enabling the control wires to be inserted. Another wire, the fixation wire, has a diameter which is larger than the difference between the screw bolt hole and the control wire diameter, so, when it is inserted in the screw bolt from the opposite direction, it will fixate the control wires. The fixation wire has to be inserted under pressure, and when this is done correctly, the wires will stay in position due to the pressure of the fixation wire.

A preliminary test showed that the grasping forceps could fully close when the wires were correctly tensioned. . The exact force which can be applied is not known yet, but even without knowing this grasping force, it can be stated that the working principle of a single part grasping forceps instrument, printed at once, is proven.

Previously, the SimulationExpress tool in SolidWorks was used to test digital drawings before printing and testing the printed parts. In the case of the alternative design bending joint geometry, the design is based on intuition rather than on simulations. However, the question arises what a simulation will show when this design is simulated and exposed to forces which imitate control wire forces. When the simulations were obtained for, among the other geometries, the triangular bending joint geometry, a force of 10 N was used to imitate the control wires. As

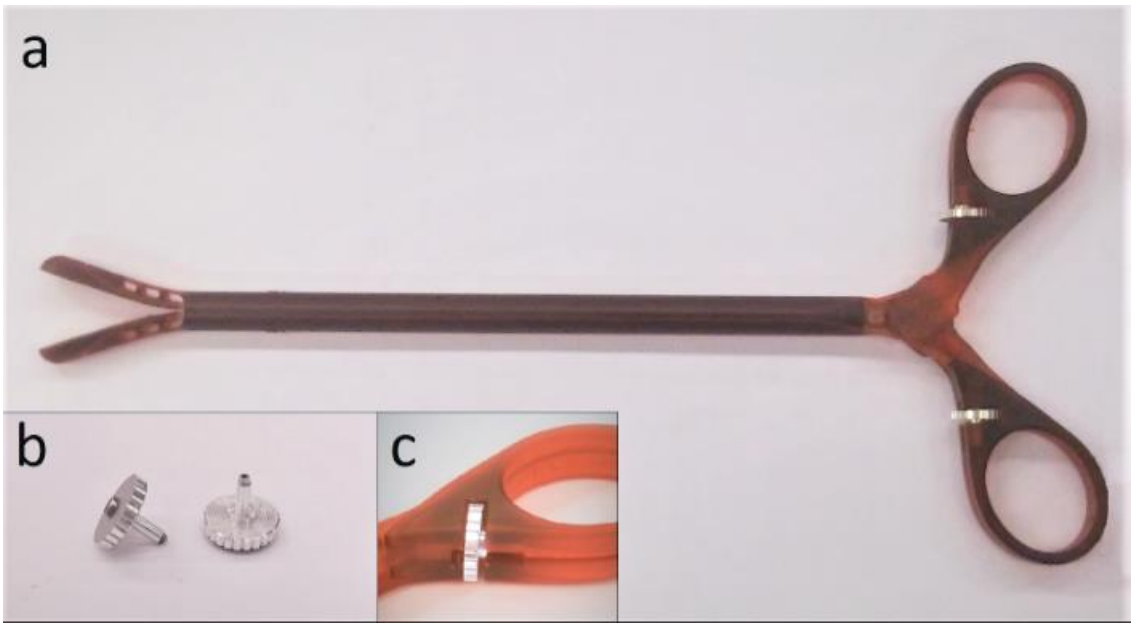

Figure 24: Final one-part instrument. (a) The instrument, (b) nuts and screw bolts in which the wires will be fixated, (c) wires fixated at one side of the control handle, the nut can be used to change the tension on the wires.

Table III: Stress, displacement and factor of safety found in the alternative design bending joint geometry, when applying a force of 10N, 5N or 2.5N imitating control wires.

	Highest stress in design [MPa]	Displacement at distal side joint [mm]	Factor of Safety
Alternative design (10 N)	96.8	19.0	0.31
Alternative design (5 N)	48.4	9.9	0.62
Alternative design (2.5 N)	24.2	5.1	1.24
Required	*< 30*	*> 6.0*	*> 2.00*

shown in Table III, in this case, the force of 10 N results in maximum stress of 96.8 MPa, which is more than three times higher than the maximum stress allowed in the design (96.8 vs. 30 [MPa]). Moreover, the factor of safety is, with more than six times lower than required, way too low (0.31 vs. 2.00). Only the displacement of the joint on the distal side is sufficient (19.0 vs. 6.0 [mm]). When the applied force to imitate the control wires is set to 5 N, the highest stress in the design is still too high (48.3 vs. 30.0 [MPa]), the factor of safety is still too low (0.62 vs. 2.00), and the displacement at the distal side of the joint is still higher than required and therefore sufficient (9.9 vs. 6.0 [mm]). When the force is again set lower, this time to 2.5 N, the highest stress finally reaches a number below the maximum (24.2 vs. 30.0 [MPa]), but the displacement at the distal side of the joint is now lower than the minimum (5.1 vs. 6.0 [mm]). The factor of safety is still too low (1.24 vs. 2.00).

It seems that according to the SimulationExpress tool in SolidWorks the alternative geometry design for the bending joint, as it is designed right now, will never be sufficient. A change in the magnitude of the applied force does not make a difference. This negative result of the SimulationExpress is in contrast with the outcomes of the manual tests of the iteratively found alternative geometry design for the bending joint. With an uncertain force, the grasping forceps closes completely, which means that the displacement at the distal side of the joint is > 6.0 mm. And the highest stress in the design should be below 30 MPa since the bending joints did not break. The real factor of safety is unknown in the design since this factor is dependent on the exact highest stress.

4.3.3. MonoFlex steerable. After the final printing iteration as described in Section 4.3.2., a minor change is added to the digital drawing in order to enable steering for the MonoFlex. In this case, the choice is made to only make the instrument steerable in one direction, just for the sake of proving the working principle of a one-part steerable surgical instrument. In future works, steering segments in other directions can be added as well. The steering segment in the instrument, as visible in Figure 25(a) is created by means of removing material out of the solid axis, in order to create a bendable thin layer in the centre of this axis, with attachments on the outer side to guide the control wires through. Figure 25(b) shows the top view of the two steering segments, one on the grasping forceps side and one on the control handle side, in the instrument. When the axis of the instrument is kept stationary between the two steering segments, and the control handle is bent in one direction relative to the stationary axis, the grasping forceps will bend into the opposite direction. This is caused by the control wires, which in one steering segment are elongated and shortened when the segment is bent, resulting in opposite reactions of the wires in the other steering segment, making it bend in the opposite direction. Figure 26(a) shows the printed version of the final one-part instrument with steering segments in the steered state.

Since the grasping mechanism works exactly the same as in the previously described final one-part instrument without steering segments (Section 4.3.2), the

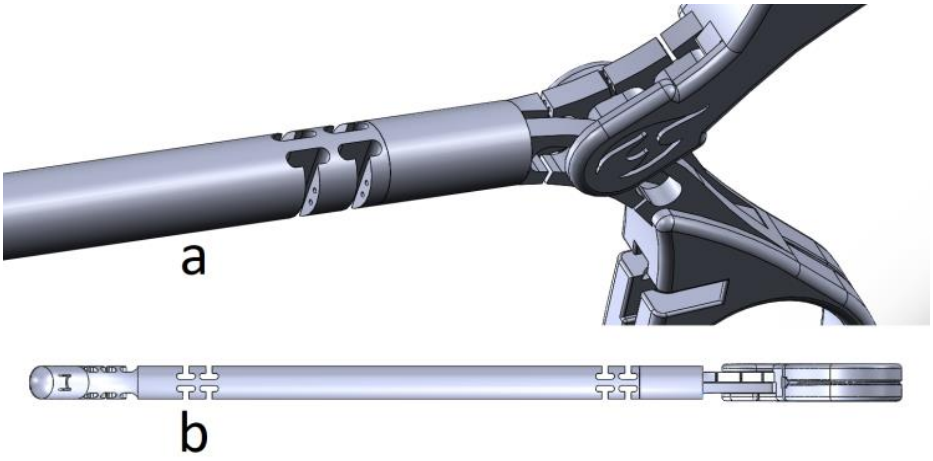

Figure 25: CAD model of instrument with steering segment. (a) Close-up, (b) top-view.

Figure 26: Final MonoFlex with steering segments. (a) Instrument in the steered state (20° (b) close-up of steering segment.

functionality of this will not be discussed again here. When it comes to the steering segments, the first observation was that these are, with a thickness of 1.5 mm, too thick to bend at all. The bending layer in the middle of the steering segments are therefore filed until a thickness of 1.0 mm is reached (Fig. 26(b)). Now, the segments can bend enough to be able to prove the working principle. The added steering segments are tested after control wires were inserted in the instrument. When the axis of the instrument was kept stationary between the two steering segments and the control handle was bent 20° relatively to the stationary axis, the grasping forceps also bend for 20° into the opposite direction. This means that the working principle of the MonoFlex is proven using this steering segment configuration. However, the steering angle is only 20° now, meaning the steering segments should be developed more elaborately in future research.

5. Testing

5.1. Introduction to the tests.

The final prototype of the MonoFlex, should pass some final tests in order to be able to verify the working principle and to see whether the requirements are met or not. Since the steering angle which can be reached with the final instrument *with* steering segments is only 20°, the choice is made not to test the steering prototype. Testing these steering segments would not add valuable results to this research because of the small steering angle, which is not large enough in the first place. Therefore, the focus of these final tests is on the final instrument *without* steering segments as described in Section 4.3.2.

Before the tests are performed, the parts to be tested are immersed in propanol for 10 minutes. During the iterative process of manually testing the different parts, it became clear that immersing the parts in propanol has a softening or plasticizing effect. This means that the parts are less brittle and more flexible. To obtain good results, the parts should withstand certain forces, which will not be the case if the parts are very brittle. However, on the other hand, it is also very important that the parts are not too flexible, making it impossible to apply required forces to grasp tissue. Although the best preparation technique – whater it is immersing in propanol or not – is not exactly known, it should be mentioned that in this research the choice is made to immerse all parts in propanol before the tests.

When it comes to the design requirement of the manufacturing process, all requirements are met. By using VAT Photopolymerization and the material EnvisionTECVR NanoCure R5, a non-assembly instrument, except adding the control wires, could be created. The dimension of the instrument only had one restriction, being the outer diameter of the distal end on the instrument which should be $\leq$ 8.0 mm. This requirement is processed in the digital drawings, and after printing the diameter is found to be 7.98 mm, meaning the requirement has been met. The required functions the instrument should include steerability, (proven in Section 4.3.3.), the ability to grasp tissue with a force of at least 10 N, and the ability of the bending joints to withstand torsion, tensile, and compression forces. The grasping force test, the torsion test, the tensile test and the compression test are described in section 5.2..

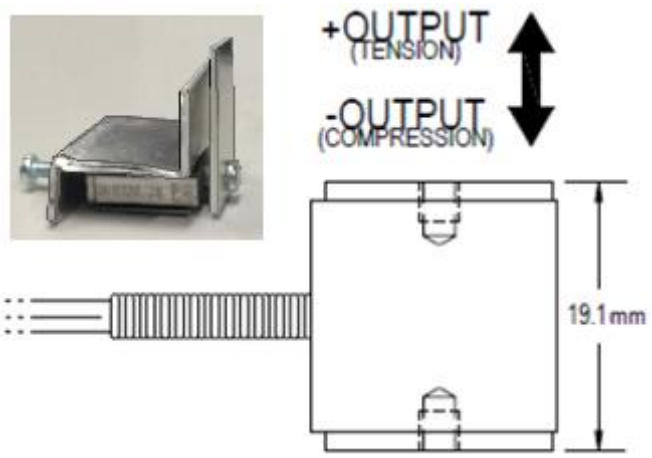

Figure 27: Front view of a mini load cell (MODEL FLLSB200 S-BEAM Junior Loadcell), with maximum output 9 N, adapted from [31]. Left above the side view of the mini load cell with aluminium extensions.

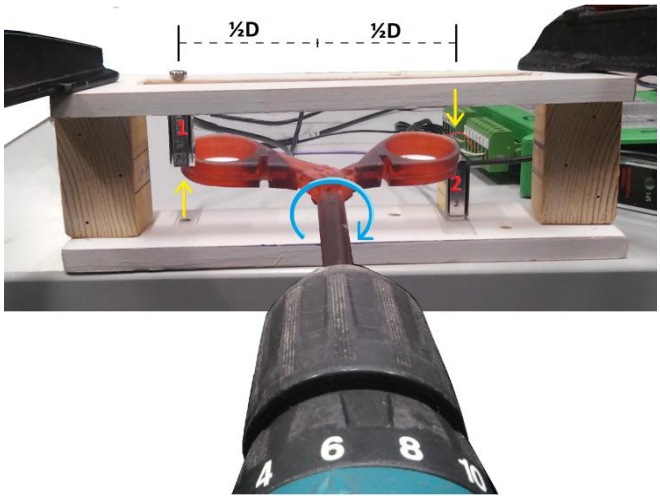

Figure 28: Results of two grasping force tests (grasping force vs. time), performed using the final one-part MonoFlex without steering segments and one mini load cell.

5.2. Execution of the tests and results.

5.2.1. Grasping force test. The most important force to be tested is the grasping force. The core function of the MonoFlex is to grasp tissue inside the body. Therefore, it is important that this force is large enough to grasp tissue at all. The test is performed by using a very sensitive mini load cell, which can measure forces up to 9 N. The two loading surfaces of the mini load cell, as shown in Figure 27, are 19.1 mm apart from each other. Since this distance is too large to be able to grasp the loading surfaces at all using the MonoFlex, some aluminium extensions are made, to make this distance smaller. The extensions basically are one flat piece of aluminium screwed on one side of the load cell, and one piece of aluminium which is bent twice, forming a z-shaped part, screwed on the other side of the load cell. In this way, the MonoFlex can easily grasp both aluminium attachment parts, which will result in a force applied on the load cell. The force being measured by the load cell is the exact force which is applied by the grasping mechanism of the MonoFlex. The test is performed twice, with the results visible in Figure 28.

Results. As can be seen, during the first test, the maximum applied force was 1.972 N, and during the second test, the maximum grasping force reached was 2.396 N. This is lower than the required grasping force of 10 N, which means the MonoFlex need more development in order to increase this grasping force.

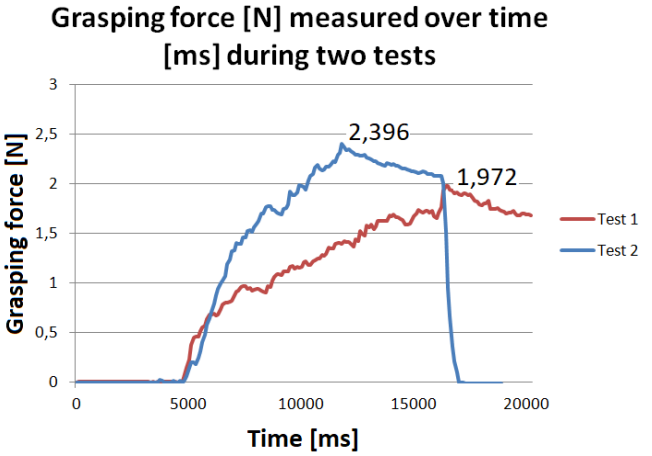

Figure 29: Set-up of torsion test. Rotary movement obtained using a battery drill (blue arrow) results in forces on two mini-load cells (yellow arrows). D is the distance between the two mini load cells.

5.2.2. Torsion test. The second test is performed to measure the maximum torsion force, which can be handled by the MonoFlex before it breaks. The test set-up (see Fig. 29) exists out of two mini load cells, facing in opposite direction, such that the instruments can be inserted between the measuring surfaces. The distance (D) between the mini load cells is adjustable and relies on the width of the instrument side to be measured. Both the grasping forceps side as well as the control handle side will be tested during this second test. The printed part to be tested is cut in two halves whereafter the instrument axis is clamped in a battery drill, which enables rotary movement. In this way, the two sides of either the control handle or the grasping forceps, are pushed against the mini-load cells that measure the exact force until the part breaks. When the average force measured by the two mini load cells is multiplied by half of the distance between the two mini-load cells, a moment can be calculated. This moment is the maximum moment that can be withstood by the bending joint of the measured instrument half.

Results. The results of the tests are shown in Figure 30, whereby Test 1 means the test performed using the control handle side of the instrument, and Test 2 is the

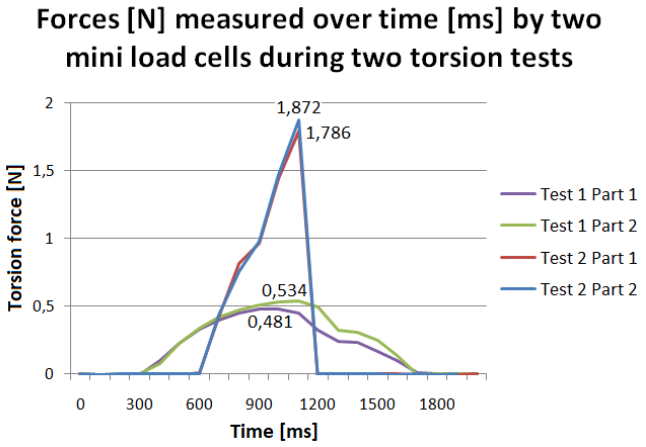

Figure 30: Results of two torsion tests, for the control handle side of the MonoFlex (Test 1) and the grasping forceps side (Test 2). Part 1 and 2 are the results measured by respectively mini load cell 1 and 2, while used simultaneously.

test using the grasping forceps side of the instrument. Part 1 and 2 are the results measured by respectively mini-load cell 1 and 2, while used simultaneously. As can be seen, the maximum values measured by the mini load cells in Test 1 are 0.481 and 0.534 N (average: 0.508 N). In Test 1, D is 82.0 mm. This means that the moments applied by the two sides of the control handle is approximately 0.508 N * (82.0 mm / 2) = 20.8 Nmm for each side. The maximum values measured by the mini-load cells in Test 2 are 1.786 and 1.872 N (average: 1.829 N). In this case, D is 36.0 mm in Test 2. This means that the moments applied by the two sides of the grasping forceps is approximately 1.829 N * (36.0 mm / 2) = 32.9 Nmm for each side. This torsion test shows that the bending joint in the grasping forceps can withstand a larger moment than the bending joint in the control handle (32.9 vs. 20.8 Nmm). One striking difference between the two tests is the way in which the graph of Test 2 goes steeply down after reaching the maximum force while in Test 1, the graph goes down more gradually. The reason for this difference lays in the fact that the bending joint on the control handle side (Test 1) did not immediately break, in contrast to the bending joint on the grasping forceps side of the instrument (Test 2). The bending joint on the control handle side kept turning while plastic deformation occurred, whereafter it also broke.

5.2.3. Tensile test. The third test is executed in order to find the maximum tensile force that can be withstood by the bending joints, both on the grasping forceps side as well as on the control handle side. During the tests, the instrument is clamped in a vise, keeping the instrument firmly in place. In both test cases, a weight carrier has been hung on the bottom side of the instrument, whereafter disc weights are placed on the

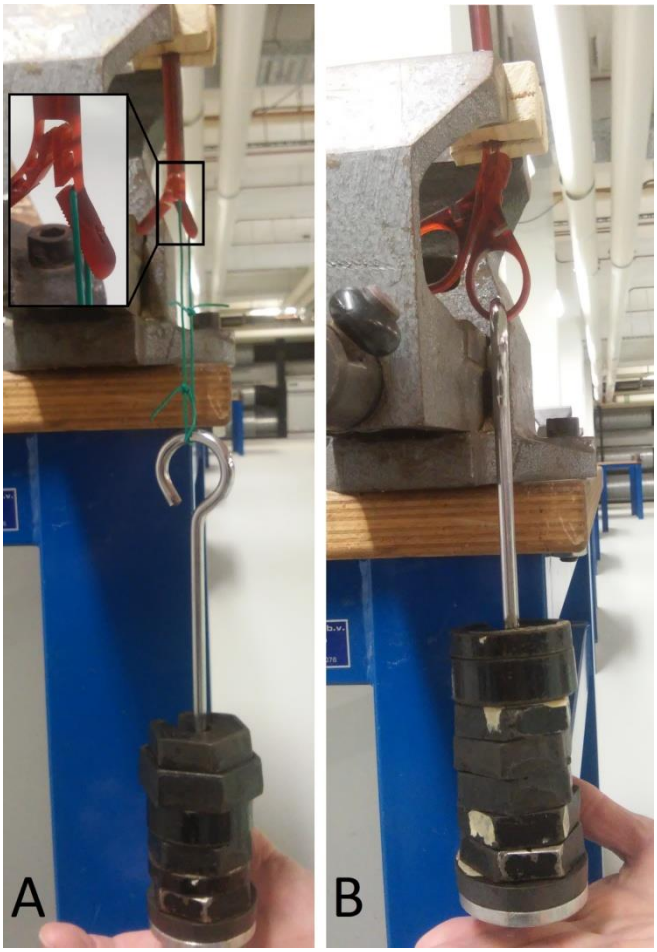

Figure 31: (a) Tensile test on the grasping forceps side of the MonoFlex, (b) tensile test on the control handle side of the instrument.

weight carrier (see Fig. 31(a) and 31(b)). Whenever the bending joint does not show any sign of fatigue, another disc weight is hung on the weight carrier to increase the weight. In both cases, all disc weights available were used in order to increase the weight.

Results. Both bending joints did not show any sign of fatigue while carrying a total weight of 2.00 kg (19.62 N), including the weight of the weight carrier. Whenever the weights were removed again, the bending joints slowly moved back to the original neutral state, without showing any signs of elongated material due to the weights.

The conclusion that can be drawn from this test is that both the bending joint on the grasping forceps side as well as the bending joint on the control handle side are relatively insensitive for tensile forces. This is as expected, since with a theoretical tensile strength of 30.0 MPa, even the smallest area on the control handle side, should be able to withstand a tensile force of 75 N or 7.65 kg (Appendix H).

5.2.4. Compression test. In the compression tests, again both the bending joint on the grasping forceps side and the bending joint on the control handle side are tested. The instrument is clamped in a vise during

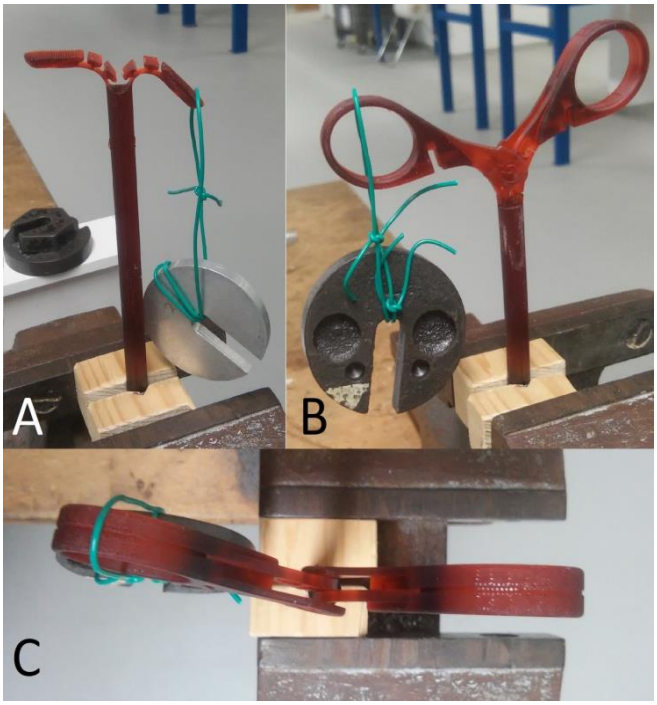

Figure 32: Compression test. (a) On the grasping forceps side of the instrument, loaded with a weight of 20 grams, (b) on the control handle side of the instrument, loaded with a weight of 150 grams, (c) top view of control handle during compression test, showing a deflection in transversal direction.

the tests. This time, the weights are hung on a cable which is hung on the top side of the instrument (see Fig. 32).

Results The grasping forceps side already bent completely after hanging up weight of 20.0 gram (0.196 N) (see Fig. 32(a)). This is in the same order of magnitude as a simulation in SolidWorks, where failure would occur at a load of 61 gram in an optimal case (Appendix I). The control handle side bent completely when a total weight of 150.0 gram or 1.472 N hung on the cable (see Fig. 32(b)). In both cases, the instrument did not return to the original neutral state, meaning plastic deformation occurred. The reason why the maximum permissible compression force on the control handle side is over seven times larger than this force on the grasping forceps side is due to the difference in bending joint configurations. On the control handle side, the control wire attachments on the bending joint, are placed on the outside of the bending joint, preventing the joint to bend overly. On the grasping forceps side, these control wire attachments are placed on the inside of the bending joint, so during the compression test, they do not provide any support. Due to the test set-up, in which the cables for the weights are hung on the outer side of the grasping forceps, this results in a moment outwards.

Another finding of the compression test is that the control handle deflects in a transversal direction, due to the non-centric design of the bending joints in the control handle. This phenomenon is also shown in Figure 32(c).

6. Discussion

The goal of the study was to design the MonoFlex, which is a one-part instrument, having the same functionality as the DragonFlex, including the steerability and the ability to grasp tissue. During the study, the focus was on the design of compliant joints, processed by using 3D-printing.

Triangular geometry printing iteration findings. After a literature search for existing compliant joint structures, digital drawings of grasping forceps were made in SolidWorks, using the SimulationExpress tool, and the most promising bending joint geometry was chosen and optimized. The first three grasping forceps printing iterations with the triangular geometry showed errors in the designs obtained during the printing process in the bending joints and the actual tips of the grasping forceps.

The first error found was the difference between digital drawings and the actual outcomes of the printer. Although the printer has high accuracy (layer thickness of 100 µm), the grooves in the printed parts were silted up, resulting in lower flexibility and functionality of the bending joint.

Secondly, the tips of the grasping forceps were warped outwards, while these should have been straight to be able to apply a grasping force. In the triangular geometry bending joint, the grooves were not equally divided while as in the digital drawings. This resulted in a structure which was highly fragile at some specific spots, and which broke almost directly after opening and closing the jaws. There are multiple reasons which could be the cause of these errors.

During the printing process, each layer was already cured with UV light. However, support structures and post-curing was necessary to obtain strong parts. When support structures were not added properly, or the post-curing was not applied correctly, this had an effect on the final parts. The structure of the triangular geometry bending joint was so thin, and the grooves were so small, that it was impossible to add support material right on the joint itself or within the grooves.

All the parts were printed in the same printing direction, with the proximal side of the instruments and parts directly on the platform of the printer, and the distal side (or tips) of the instruments and parts

pointing downwards. If the parts were printed in another printing direction, the final part possibly looked different, since the gravity would work in another direction relative to the part. Another cause for the errors found in the first three printing iterations could lay in the fact, that incompletely cured parts could build internal stresses due to the anisotropy of the material and temperature differences between printing layers during the printing process. In particular, the warped grasping forceps tips could be a result of internal stresses. The tips were quite thin, and stresses which were possibly present inside the material or between printed layers could warp this thin structure. In the next iterations, this problem was solved by making the tip larger, twice long, and with less sharp edges. In case of internal stresses, a larger tip would logically be more difficult to warp compared to a small and thin tip.

Single bending layer geometry printing iteration findings. In the grasping forceps with alternative geometry bending joint (fourth and fifth printing iterations), also some different errors occurred, besides the warped tip. The T-shape attachments, required to guide the control wires through, were printed inaccurately due to a lack of support material. During the fifth printing iteration, an addition of support material solved this error, making the parts look like the digital drawing. This step in the printing process particularly proves the need for properly placed support material when using VAT Photopolymerisation as printing technique for complex structures. However, removing the support structures after printing takes relatively much time, which is a drawback when one of the main goals of this research is to make these one-part instruments to save manufacturing and assembly time. This problem could possibly be prevented when another design than the T-shape attachments were used to guide the control wires, not requiring support material. An example of a small but effective change of the attachment parts would be using a L-shape instead of a T-shape, where the horizontal bar of the letter T, basically is shifted to one side, creating an upside-down L. One of the sides could not be printed without support material, so when this side is shifted to the adjacent attachment part, the problem is solved. However, during this research the choice is made to continue using the T-shape since it is a good example of an interesting side issue that could occur when printing medical instruments that contain complex structures. Moreover, despite the issue of the required support structures, the functionality of the grasping forceps mechanism with alternative geometry bending joint was more promising than the triangular geometry bending joint grasping forceps, in contrast to what the SimulationExpress tool in Solidworks predicted.

Control handle printing iteration findings. The control handle, as designed after two printing iterations, showed promising results on first hand. When it comes to the functionality, it allows the instrument user to open or close the grasping forceps. However, some limitations can be mentioned as well: the weakness when it comes to torsion or compression forces. Apparently, the bending joints on the control handle side are too small or thin to withstand these forces. Moreover, the fact that these bending joints are not designed centrally on the instrument shaft, allows the control handle sides to deflect in a transversal direction when exposed to a compressive or torsion force. The effects of exposing the control handle to different forces are encountered during the tests of the final instrument.

Issues with SimulationExpress tool. During the manual tests, performed after each printing iteration, the parts acted different than expected. It seems that the SimulationExpress is not as accurate as required in the way it is used for this research. Of course, simulations always will be different compared to real life, but nowadays, also simulation techniques are highly optimized. The problem, in this case, could be caused by the lack of information regarding the properties of the material EnvisionTECVR NanoCure R5. The SimulationExpress tool requires more material properties to be able to simulate a situation accurately. For example, the Poisson's ratio is one of these required material properties, which in this case is unknown. The Poisson's ratio of a similar material as the material used in this research, was found and said to be 0.40 [32]. Logically, if all material properties were inserted correctly in the SimulationExpress tool, the outcome could have been different. Also, the tool assumes the material to be isotropic, while this might not be the case, since the parts are printed in layers.
Another issue that occurred while using the SimulationExpress, was that forces, which were applied in a certain direction, did not move along with the bending joints in the design, but stayed in exactly the same (initial) direction during the whole simulation. In other words, when a pre-bent grasping forceps jaw became more horizontal after applying the simulation force, the force did not become horizontal at all, but stayed as slanted as the forceps jaw in initial

state. The simulation would have been more accurate if these forces bent along with the grasping forceps.

A third questionable issue in SolidWorks is the limited mesh size. Since the mesh density determines the precision of the simulation solution, it is necessary to have the right mesh density. Especially in cases where sharp edges or cuts could cause stress concentrations, this is highly important. In this research the smallest mesh size possible was used, though this mesh size is still relatively large compared to the structure. However, when the minimal mesh size was enlarged (doubled), the results of the simulations were only slightly different. This means that it is likely, that with the smallest mesh size, the real values of stresses and displacements were approached fairly well.

Test findings. The final instrument, existing out of a grasping forceps attached to the control handle, was tested during four tests; (1) the grasping force test, (2) the torsion test, (3) the tensile test and (4) the compression test.

According to the design requirement, the grasping forceps should be higher than 10 N, since the average force that is used to grasp tissue during surgeries lays between 10 – 20 N. However, the required force to softly grasp liver tissue for example, is only 2-4 N [30]. During the grasping force test, the maximum force which could be applied with the grasping forceps was found to be 2.396 N, which is way lower than the required force. This force could be enough to lift light-weight objects or softly grasp tissue, but it is certainly not large enough to lift heavier objects. A combination of the strength of the instrument and the tension on the control wires is responsible for the grasping force. When, in future, these will be improved and made stronger, the grasping force should be higher as well.

The torsion tests on both sides of the instrument resulted in two maximum moments which could be withstood by the sides. A maximum moment of 20.8 Nmm was obtained for both sides of the control handle, while both jaws of the grasping forceps withstood a maximum moment of 32.9 Nmm, which is still quite small. The grasping forceps is more resistant to torsion forces compared to the control handle. As mentioned earlier, this probably is due to the differences in bending joint designs, whereby the bending joints on the grasping forceps side are more centrally located on the instrument shaft and wider as well compared to the bending joints on the control handle side. However, still both the grasping forceps as well as the control handle cannot resist quite large moments, which implies this needs some more investigation and development as well. Especially in the medical field and during surgeries it is highly important that instruments have a high reliability and durability.

The compression test showed similar results as the previously mentioned tests. Under low forces, 0.196 N (20 gram) for the grasping forceps and 1.471 N (150 gram) for the control handle, plastic deformation occured. In this test, fatigue was clearly visible since the parts were completely bent and did not move back to the original neutral state. This is another sign of the lack of durability of the instrument, and this should be solved as well by strengthening the bending joints. A limitation of the compression test was that the forces used to obtain compression do not solely induce pure compression, but rather a moment around the bending joint. This is due to the pre-bent printed joint, which did not allow pure compression in longitudinal direction of the joint. The results however, were as expected, since a simulation with the same test setup showed that failure would occur on the grasping forceps side after applying a force of 0.6 N, which is the same order of magnitude.

When it comes to the tensile test, it is striking how the obtained results were so much better compared to the other tests, although this was also predictable. Both the grasping forceps as well as the control handle did not show any sign of fatigue when exposed to relatively large tensile forces. The largest force which could be tested with the available equipment, was 19.62 N (2.00 kg) for both sides of the instrument. In the most optimal case in theory, the instrument should be able to withstand tensile forces upto 108.79 N (11.09 kg).

Proven working principle. Where three out of four tests showed results which make clear, the MonoFlex still needs development and improvement when it comes to the strength and durability, the working principle of a one-part controllable instrument is proven. We have shown the MonoFlex can grasp (light-weight) objects without the need for assembly except adding the control wires. Moreover, some steering segments were added in the last printing iteration, which showed it is possible to make a one-part steerable instrument, although the steering segments only allow steering in one direction, where the DragonFlex is steerable in two directions. Thus, the steering mechanism is not perfect yet and needs development as well, but the working principle – a one-part steerable instrument – has been proven.

Reflection on some design choices. The focus in this research was on the development of compliant joint structures for the use of a medical instrument. From the start on, a selection of bending flexure joints, which already have been used in MIS instruments, was used to continue the iterative process of designing, printing and testing to improve these joints and make them printable. However, outside the MIS field, many more bending flexure joints exist, which possibly also can be used in MIS instruments. Examples of such alternative compliant joints are visible in Figure 33.

To simplify the control mechanism of the grasping forceps, the choice was made to print the jaws of the mechanism in pre-bent state. Now only an active control action was required when the grasping forceps had to close. This implies that when no active force was applied to the control handle, the grasping forceps would open. Where this, from an technical point of view, may be useful, from an medical point of view this might become a important safety issue. When, for example, one of the control wires unexpectedly snaps, the grasping mechanism will automatically go to its neutral position, which in this case is the opened state. When the instrument is inserted in a patient during a MIS procedure, and this happens, the clinician is probably not able to remove the instrument safely. The internal tissue of the patient could be seriously harmed. From this point of view, a straight printed part would be more safe.

Another point of interest, is the choice of material. Since this material showed promising results in previous similar researches, the choice was made to use this non-biocompatible material. However, from an environmental and safety point of view, it would be more justified to use biocompatible or in future even biodegradable materials.

Future research. Apparently, the designs made in SolidWorks and the simulations obtained with the SimulationExpress tool were significantly different from the actual printed parts. Where the triangular geometry seemed very promising, and the alternative single layer geometry seemed to be too fragile, the opposite was true. As mentioned in section 3.2.1., theory already showed that sharp edges or cuts are not recommended to be used, since they can act like cracks in the material, which propagate when stresses are applied. In this research, this theory has been proven again. Also, the parts looked in some cases quite different from the digital drawing. Therefore, it would be really interesting and valuable to investigate the

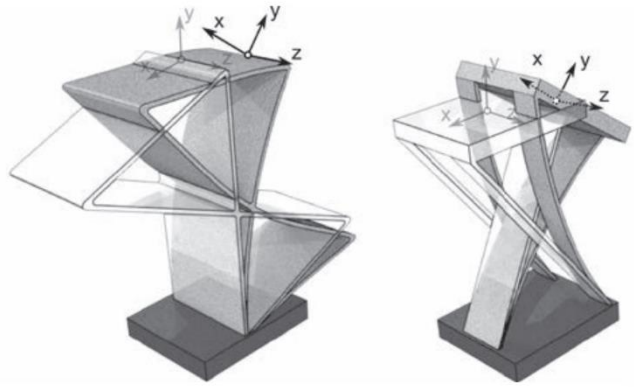

Figure 33: Deflected flexural building blocks, adapted from [35].

actual reasons behind these differences between the software and the printed parts.

The question however rises: If the perfect compliant joint can be designed and printed as designed, will this be a good solution to be used in medical applications anyway? Where the final version of the MonoFlex in this research has proven the working principle of a non-assembly surgical instrument, created by means of 3D-printing, the instrument is still unsafe for medical applications. The largest drawback of the MonoFlex is the fatigue of the bending joint, which is not present in the DragonFlex since the DragonFlex does not use compliant joints. This weakness and fragility of the instrument either have to be tackled or the conclusion must be drawn that compliant joints in MIS instruments are just not safe enough. Because of the lack of durability, more research has to be done into making the instrument stronger. The cause can possibly lay in the fact that only one material is used during this research, where a combination of multiple materials with different material properties, could enable a design which is more durable and reliable. Of course, it will be a challenge to design such an instrument and make it printable using different materials by a single printer. Another reason for the lack of durability could again be the printing direction. The force applied by the control wires is perpendicular to the printed layers, which in theory is the weakest direction to put a force on. It could be interesting to print the instrument in different directions, apply the same force tests as described above, and see what the differences are. If the MonoFlex is made stronger, the highest grasping force will also be higher, making the instrument more useful for surgical purposes.

When comparing the MonoFlex with the DragonFlex, the last one still seems to be more effective and durable at this stage. However, the author thinks there are still interesting opportunities to improve the MonoFlex mechanism as it is right now,

with the chance to introduce an innovative MIS instrument which can save time and costs over the long term. Therefore, research in compliant joint structures for MIS instruments should not be disregarded, it even could be useful for other purposes or other medical applications than MIS.

Another relevant research topic besides the compliant joint structure itself, would be the influence of propanol on material properties. The material EnvisionTECVR NanoCure R5 hardens under light, and softens becoming more flexible when submerged in propanol. In what order the material becomes more flexible or less fragile, as well as the dependence on submerging time is unclear. This information would be valuable and relevant for researchers who also use this material type of resin in the future.

The last recommendation for future research is to develop the steering mechanism and making the instrument steerable in multiple directions. The more degrees of freedom the instrument has, the bigger the impact in the medical field, especially when the instrument is designed for Minimally Invasive Surgery purposes, as it is in this case.

7. Conclusion

In this study, MonoFlex, a 3D-printed one-part instrument, was designed based on the DragonFlex grasping forceps. Having the same functionality as the DragonFlex, the fundamental requirement was the assembly of only the control wires in a non-assembly instrument body. The prototype was developed using SolidWorks and its SimulationExpress tool. The iterative design process resulted in final prototypes, with and without steering segments. After performing several force tests, the instrument is found to be too undurable as it is right now. However, the main goal was to develop an one-part grasping instrument, which has been accomplished, and therefore the working principle of a one-part 3D printed grasping prototype is proven by this research. Some challenges still have to be overcome when it comes to the strength of the instrument. Future research should focus on making the instrument stronger, for example by using multiple materials. Although the DragonFlex seems to be a more reliable solution for MIS instruments than the MonoFlex at this stage, the MonoFlex surely has potential. Depending on 3D printing techniques, which are also continuing to develop at a high speed, it is only a matter of time, and the successors of the MonoFlex will conquer the MIS field with instruments being durable, cheap, reliable and safe for both clinician and patient.

Bibliography

[1] Braga, M., Vignali, A., Gianotti, L., Zuliani, W., Radaelli, G., Gruarin, P., Dellabona, P., and Carlo, V. D., 2002, "Laparoscopic Versus Open Colorectal Surgery: A Randomized Trial on Short-Term Outcome," Ann. Surg., 236(6), pp. 759–767.

[2] Breedveld, P., Stassen, H. G., Meijer, D. W., and Jakimowicz, J. J., 1999, "Manipulation in Laparoscopic Surgery: Overview of Impeding Effects and Supporting Aids," J. Laparoendosc. Adv. Surg. Tech., Part A, 9(6), pp. 469–480.

[3] Khoorjestan, S. M., Najarian, S., Simforoosh, N., and Farkoush, S. H., 2010, "Design and Modeling of a Novel Flexible Surgical Instrument Applicable in Minimally Invasive Surgery," Int. J. Nat. Eng. Sci., 4(1), pp. 53–60.

[4] Minor, M., and Mukherjee, R., 1999, "A Mechanism for Dexterous End-Effector Placement During Minimally Invasive Surgery," ASME J. Mech. Des., 121(4), pp. 472–479.

[5] Velanovich, V., 2000, "Laparoscopic versus Open Surgery," Surg. Endosc., 14(1), pp. 16–21.

[6] Arrow Medical, 2012, "Bruder 5 mm Ø Laparoscopic Instruments," http://www.arrowmedical.com /sites/default/files/5MM%20LAP%20DISSECTOR,%20GRASPER,%20BIOPSY%20FORCEPS%20%26%20SCISSORS.pdf

[7] Breedveld, P., 2010, "Steerable Laparoscopic Cable-Ring Forceps," ASME J. Med. Devices, 4(2), p. 027518.

[8] Breedveld, P., Stassen, H. G., Meijer, D. W., and Stassen, L. P. S., 1999, "Theoretical Background and Conceptual Solution for Depth Perception and Eye–Hand Coordination Problems in Laparoscopic Surgery," Minimally Invasive Ther. Allied Technol., 8(4), pp. 227–234.

[9] Jelınek, F., Pessers, R., and Breedveld, P., 2014, "DragonFlex Smart Steerable Laparoscopic Instrument," ASME J. Med. Devices, 8(1), p. 015001.

[10] Jelınek, F., Diepens, T., Dobbenga, S., van der Jagt, G., Kreeft, D., Smid, A., Pessers, R., and Breedveld, P., 2015, "Method for Minimising Rolling Joint Play in the Steerable Laparoscopic Instrument Prototype DragonFlex," Minimally Invasive Ther. Allied Technol., 24(3), pp. 181–188.

[11] Jelınek, F., Gerboni, G., Henselmans, P. W. J., Pessers, R., and Breedveld, P., 2015, "Attaining High Bending Stiffness by Full Actuation in Steerable Minimally Invasive Surgical

Instruments," Minimally Invasive Ther. Allied Technol.,24(2), pp. 77–85.
[12] EnvisionTEC 2014, "Perfactory, Material R5 and R11," http://media.envisiontec.com/envisiontec/wp-content/uploads/2014/04/MK-MTS-R5R11-V01-FN-EN.pdf
[13] Jelinek F, Arkenbout EA, Henselmans PWJ, Pessers R, Breedveld P, (2015). *Classification of Joints Used in Steerable Instruments for Minimally Invasive Surgery—A Review of the State of the Art*. Journal of medical devices: Vol. 9 / 010801-1.
[14] Parrott, D. A., Krupp, B. T., Gillum, C. L.,Matice, C. J., andMingione, L. P., 2012, "Articulating Laparoscopic Surgical Instruments," WOPatent No. 2012/058213.
[15] Banik, M. S., Boulais, D. R., Couvillon, L. A., Chin, A. C. C., Anderson, F. J., Macnamara, F. T., Fantone, S. D., Braunstein, D. J., Orband, D. G., Saber, M., Hunter, I. W., Coppola, P. A., Kirouac, A. P., Clark, R. J., Wiesman, R. M., Mason, T. J., Mehta, N. R., and Greaves, A. E. R., 2013, "Articulation Joint," EP Patent No. 2,617,350.
[16] Kortenbach, J. A., Gottlieb, S., Smith, K. W., Slater, C. R., and Bales, T. O., 2003, "Rotatable and Deflectable Biopsy Forceps," U.S. Patent No. 2003/0195432.
[17] Ouchi, T., 2010, "Treatment Tools for Endoscope," U.S. Patent No. 7,857,749.
[18] Lee, W., Chamorro, A., Ailinger, R., and Meglan, D., 2010, "Robotically Controlled Surgical Instruments," U.S. Patent No. 7,699,835.
[19] Chong, E., 2008, "A Catheter Steering Device," U.S. Patent No. 2008/0319418.
[20] Erhard, M., 2005, "Laparoscopic Instrument," EP Patent No. 1,584,293.
[21] Griffiths, J. R., 2013, "System and Method for an Articulating Distal End of an Endoscopic Medical Device," U.S. Patent No. 2013/0150831.
[22] Knodel, B. D., Thompson, B., Manoux, P. R., and White, N. H., 2012,"Method for Treating Tissue With an Articulated Surgical Instrument," U.S. Patent No. 2012/0061446.
[23] Kovac, T. J., and Wei, M. F., 2003, "Endoscopic Surgical Instrument for Rotational Manipulation," U.S. Patent No. 6,663,641.
[24] Lenker, J. A., and Pool, S. L., 2013, "Steerable Endoluminal Punch," WO Patent No. 2013/158354.
[25] Lyons, E., Rose-Innes, D. J., and Brewer, R. J., 2012, "Surgical Instrument," U.S. Patent No. 8,241,320.
[26] Stone, K. T., Walters, T. M., and Kaiser, R. A., 2007, "Steerable Suture Passing Device," U.S. Patent No. 2007/0038230.
[27] Verbeek, M. A. E., 2012, "Steerable Tube, Endoscopic Instrument and Endoscope Comprising Such a Tube, and an Assembly," WO Patent No. 2012/173478.
[28] Viola, F. J., 2013, "Surgical Stapler Having an Articulation Mechanism," U.S. Patent No. 2013/0032627.
[29] Additive Manufacturing Research Group, 2018, "About additive manufacturing: VAT Photopolymerisation", Loughborough University, UK.
[30] Yamanaka, H., Makiyama, K., Osaka, K., Nagasaka, M., Ogata, M., Yamada, T., and Kubota, Y., (2015). "Measurement of the Physical Properties during Laparoscopic Surgery Performed on Pigs by Using Forceps with Pressure Sensors", Advances in Urology, DOI: 10.1155/2015/495308.
[31] Feteris Components B.V.. MODEL FLLSB200 S-BEAM Junior Loadcell. Drawing Number: FI 1041-C.
[32] Polymer Properties Database (2015). Typical Poisson's ratios of polymers at room temperature. Obtained from: http://polymerdatabase.com/polymer%20physics/Poisson%20Table2.html
[33] Tille, C. Process Errors and Aspects for Higher Resolution in Conventional Stereolithography. Caesar research center Ludwig-Erhard-Allee 2, 53175 Bonn/Germany
[34] Kivelä, L., (2019). 3D print warping – 10 easy fixes for PLA, PETG & ABS. Obtained from: https://all3dp.com/2/3d-print-warping-what-it-is-how-to-fix-it/
[35] Naves, M., Aarts, R., Brouwer, D., (2017). Large Stroke Flexure Hinges. Mikroniek, 57(3), pp. 5-13.
[36] Roylance, D., (2001). Introduction to Fracture Mechanics. Department of Materials Science and Engineering: Massachusetts Institute of Technology Cambridge, MA 02139

Appendices

Appendix A: Dog bone test results

The dog bone tests exist out of six tests of identical dog bones as visible in Figure A.1. These dog bones also underwent a propanol treatment, similar to the test parts in Chapter 5. The cross-section of the smaller area in the middle of the dog bone is of size 4.0mm x 9.95mm.

Figure A.1: Dog bone as used in five dogbone tests.

To be able to calculate the Young's modulus, the direction coefficient of the linear track till the yield stress has to be calculated. At the yield stress, elastic deformation turns into plastic deformation. Because of all the results do not show a clear yield point, the linear track is estimated manually. It seemed that in all tests, the track seems linear between 1 MPa and 5 MPa. The values closed to 1 MPa and 5 MPa in the tests plus the strains obtained by applying these pressure are used to calculate the Young's modulus. The average of the Young's moduli calculated using the six tests is found to be:

$$\mathbf{E_{average}} = \frac{(E1+E2+E3+E4+E5+E6)}{6} = \frac{6{,}285\ GPa}{6} = \mathbf{1{,}048\ GPa}$$

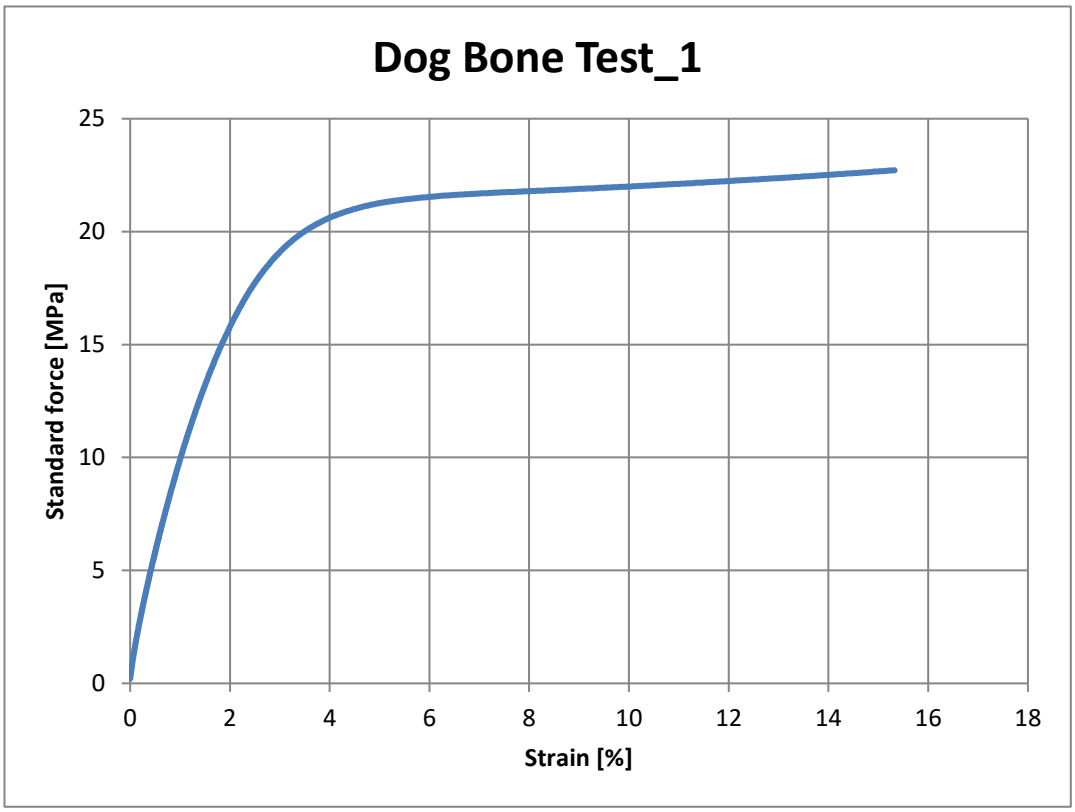

$$E_1 = \frac{\sigma(5MPa)-\sigma(1MPa)}{\varepsilon(5MPa)-\varepsilon(1MPa)} = \frac{4{,}01\ MPa}{0{,}363\ \%} = 1{,}105\ \text{GPa}$$

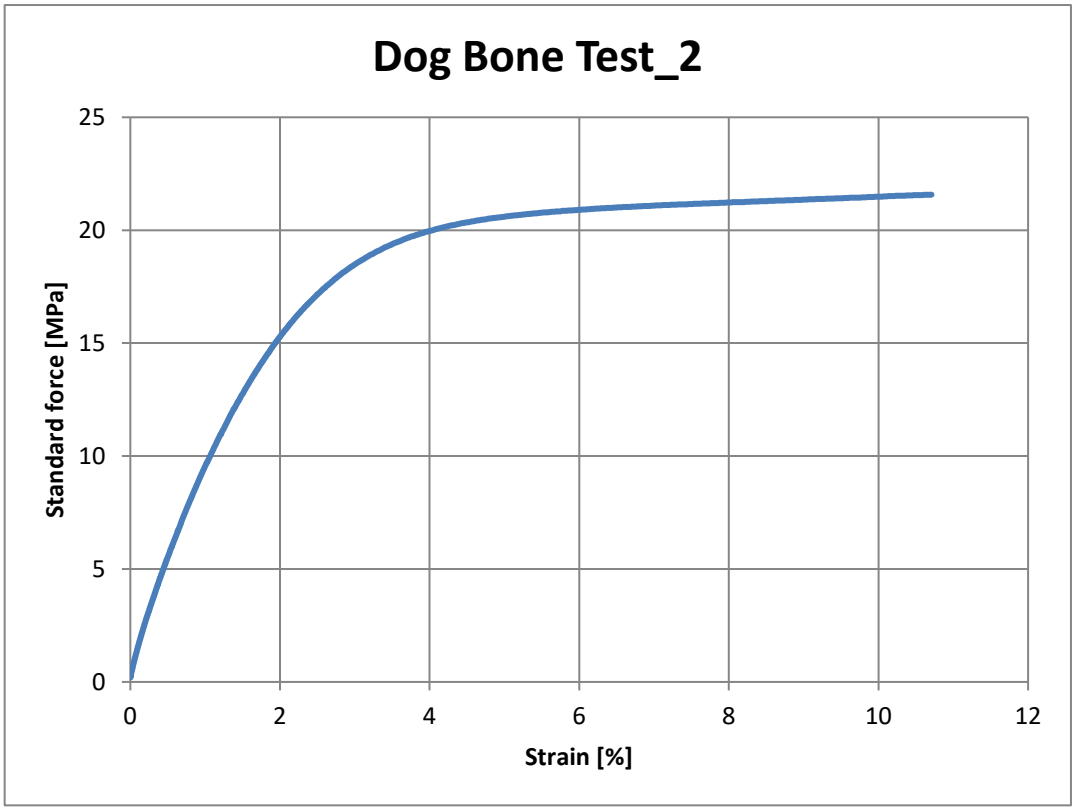

$E_2 = \frac{\sigma(5MPa) - \sigma(1MPa)}{\varepsilon(5MPa) - \varepsilon(1MPa)} = \frac{3{,}99\ MPa}{0{,}384\ \%} =$ 1,038 GPa

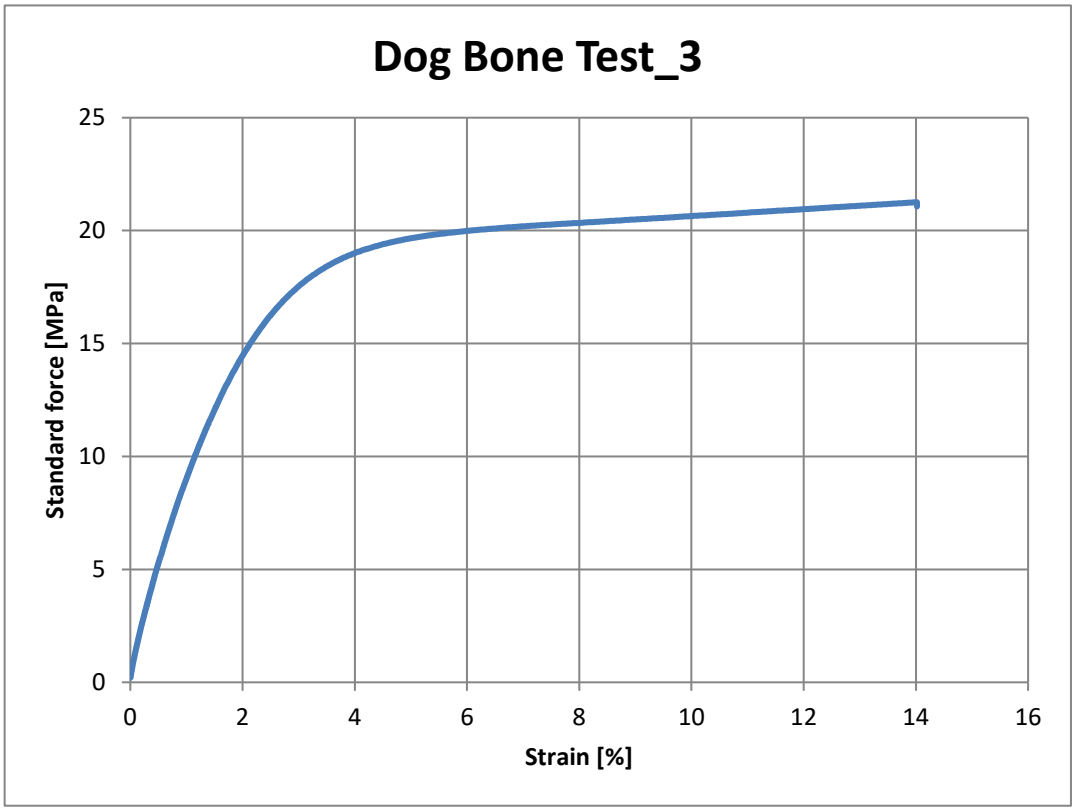

$E_3 = \frac{\sigma(5MPa) - \sigma(1MPa)}{\varepsilon(5MPa) - \varepsilon(1MPa)} = \frac{3{,}99\ MPa}{0{,}407\ \%} =$ 0,982 GPa

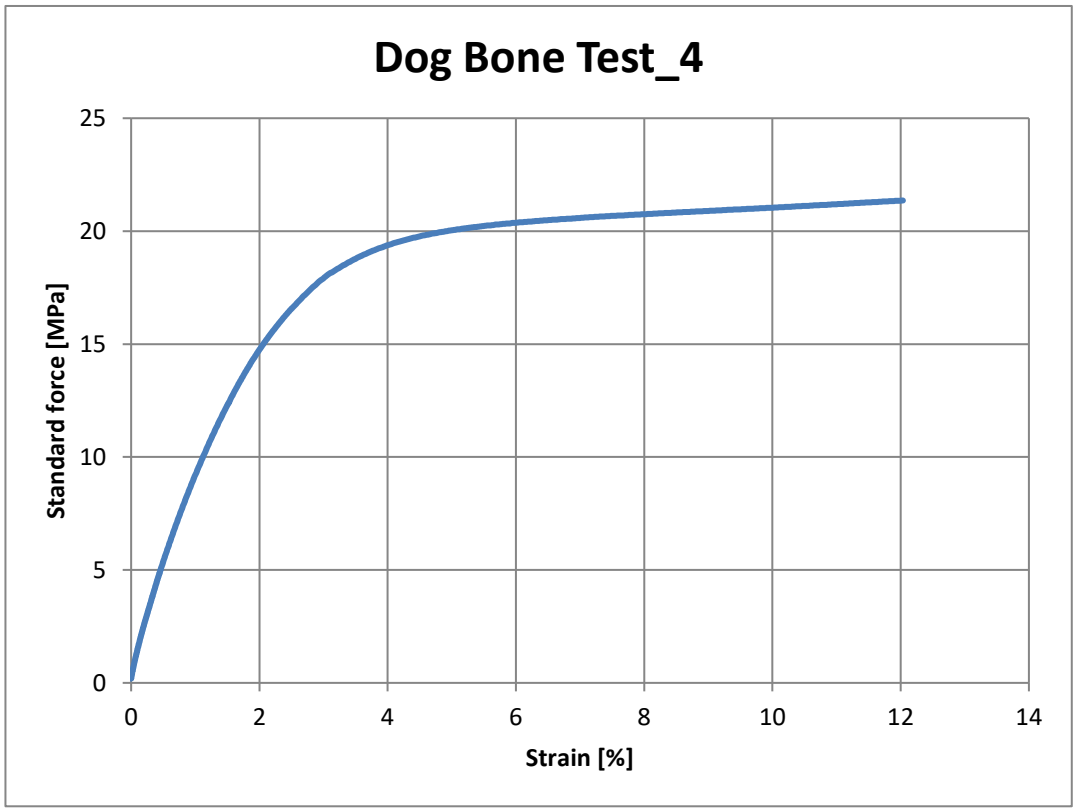

$E_4 = \frac{\sigma(5MPa) - \sigma(1MPa)}{\varepsilon(5MPa) - \varepsilon(1MPa)} = \frac{3{,}99\ MPa}{0{,}399\ \%} =$ 1,000 GPa

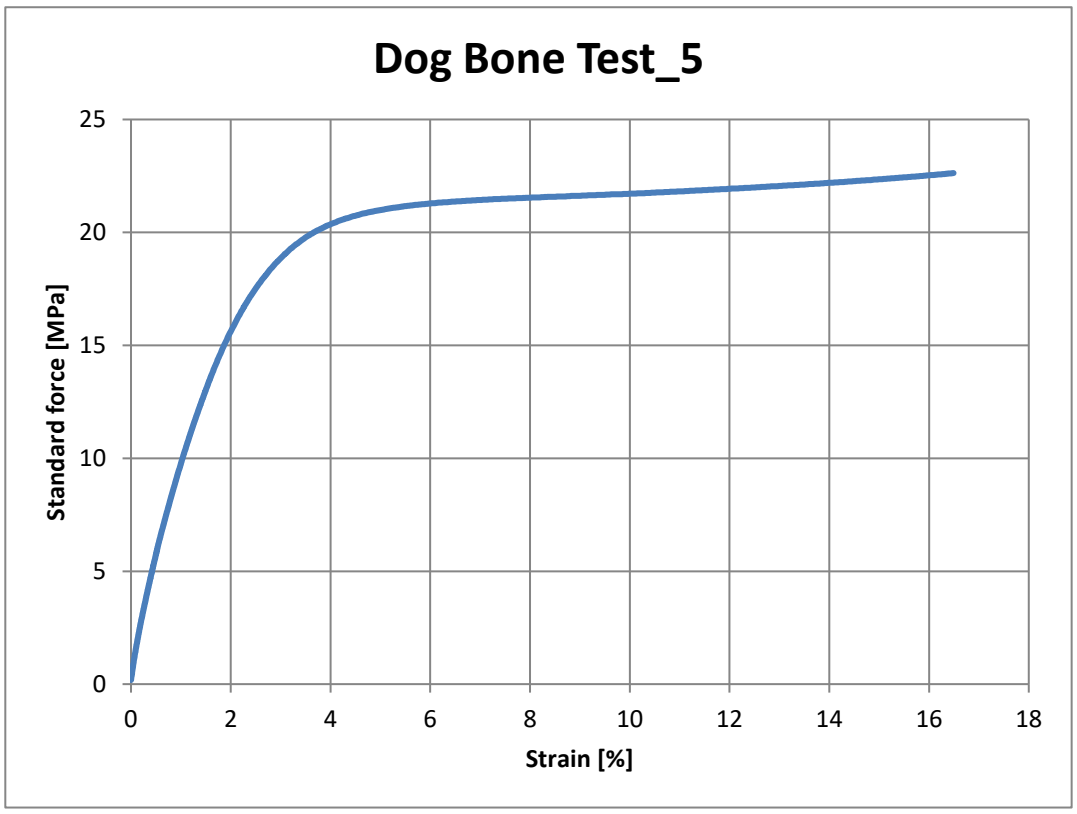

$E_5 = \frac{\sigma(5MPa) - \sigma(1MPa)}{\varepsilon(5MPa) - \varepsilon(1MPa)} = \frac{4{,}01\ MPa}{0{,}368\ \%} =$ 1,088 GPa

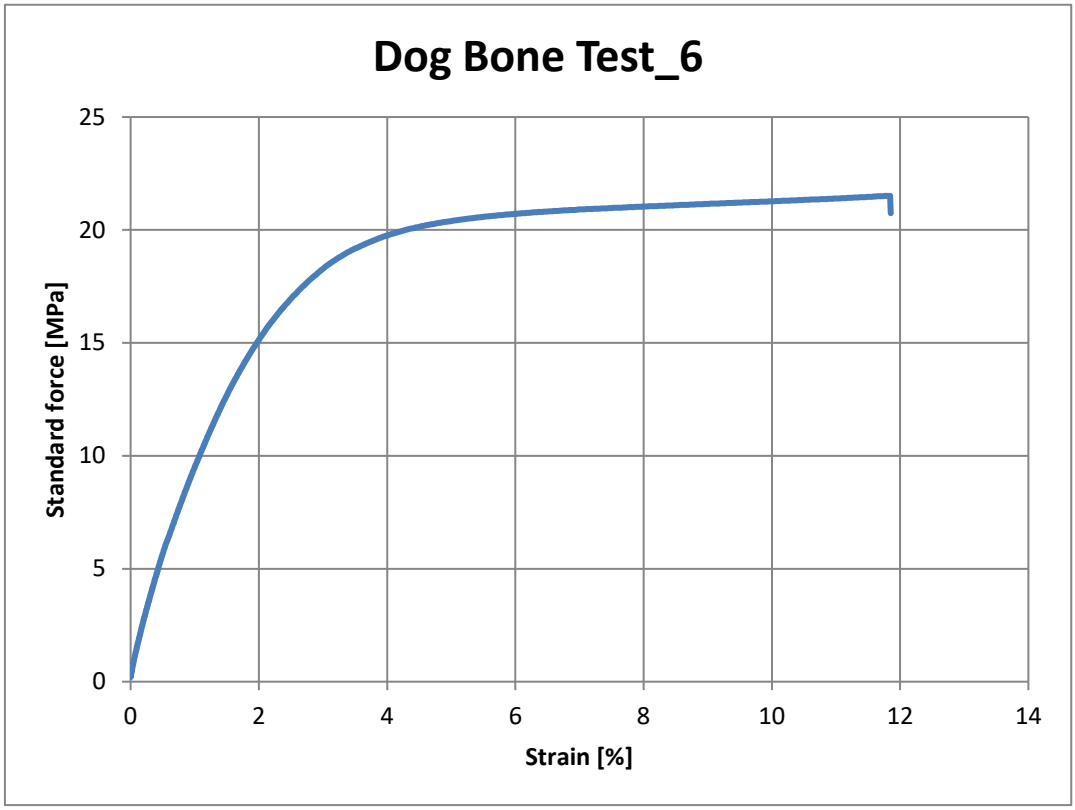

$$E_6 = \frac{\sigma(5MPa) - \sigma(1MPa)}{\varepsilon(5MPa) - \varepsilon(1MPa)} = \frac{4{,}00\ MPa}{0{,}373\ \%} = 1{,}072\ \text{GPa}$$

Appendix B: SolidWorks settings in SimulationExpress Tool

As visible in Table B, the properties of the material EnvisionTECVR NanoCure R5 resin are used during the simulations in SolidWorks. For the Young's Modulus (Elastic Modulus), the value as calculated in the Dog Bone Tests (appendix A) is used.

Table B: SolidWorks settings during simulations.

Property	Value	Unit
Mesh global size	0.355	mm
Mesh accuracy	0.0177	mm
Elastic Modulus	1.048	GPa
Poisson's ratio	0.4	N/A
Mass density	1000	Kg/m^3
Tensile strength	31.0	MPa
Yield strength	30.0	MPa

Appendix C: Problem of stress concentrations and limited mesh sizes

When a force on an area is evenly distributed, an object is stronger. If the area is reduced on a specific spot, this results in an localized increase in stress. When an object has grooves or cut in a triangular shape, for example, the corners will most probably also show stress concentrations. These specific stress concentration spots are likely to fail, and should therefore be tested and simulated most accurately.

In a FEM simulation, such as in the SimulationExpress tool in SolidWorks, the mesh density determines the precision of the solution. The default setting in theory should provide an accurate deformation solution and a reasonably accurate stress distribution. However, when a finer mesh is used, this will improve the stress results in local areas (Fig. C.1). The problem with the SimulationExpress tool is that the mesh size is limited. The smallest mesh size possible (SolidWorks software obtained with student license) is 0.355 ± 0.0177 mm. This mesh size is used to conduct the simulations and continue the research.

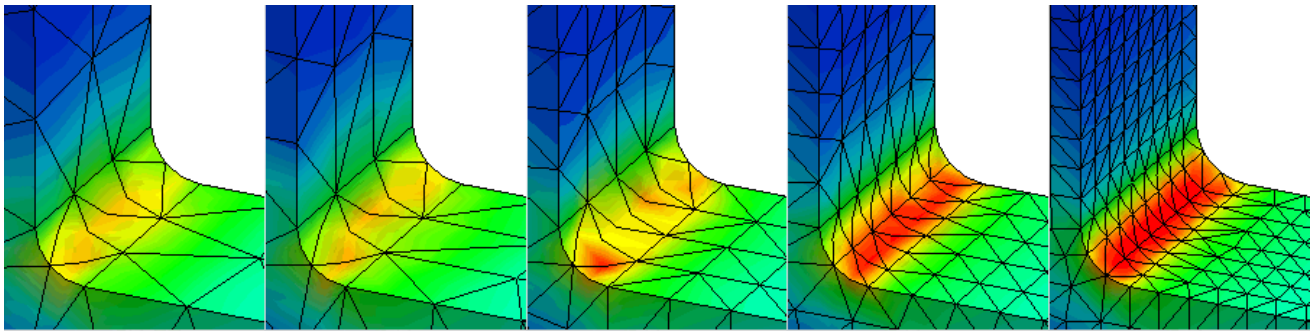

Figure C.1: Different meshsizes from left (coarse mesh) to right (fine mesh). In the coarse meshes, the details are lost.

Appendix D: Block tests

The basic geometries of the four tested blocks are visible in Figure D.1.The dimensions A, B and C are all 1.0 mm.

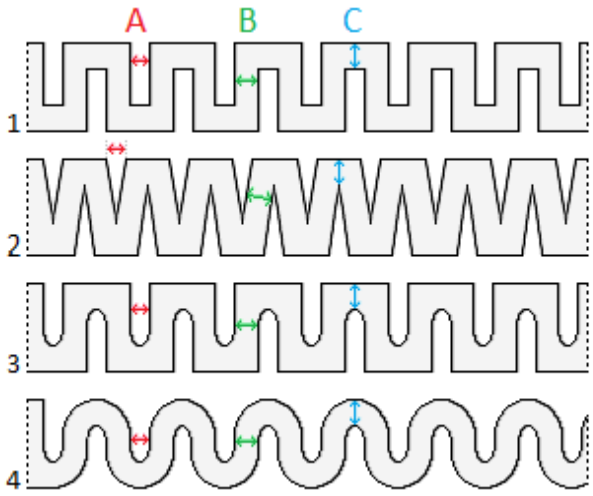

Figure D.1: Rectangular, triangular, cylindrical, and wave geometries, with the gap width (A), material width (B), and material height (C) kept constant.

These geometries are implemented in blocks with similar cross-sections (8.0 x 4.0 mm^2). Images of these blocks are visible in Figure D.2. The blocks are constrained on one side and an evenly distributed force of 10 N is applied on the opposite side. The results obtained after performing the block tests are visible in Table D. Figure D.3 shows the blocks after applying the forces.

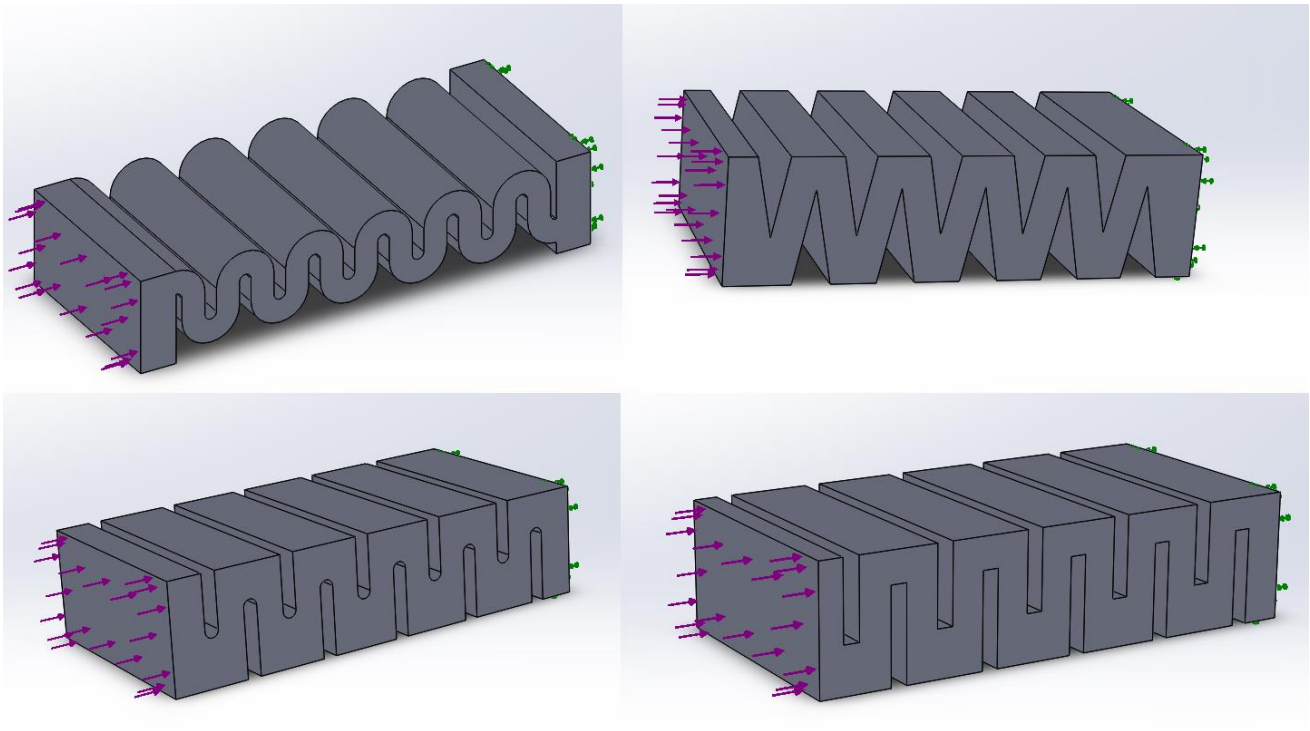

Figure D.2: Blocks with four different geometries as used for the block tests. The blocks are constrained on the right side and an evenly distributed compression force of 10 N is applied on the left side.

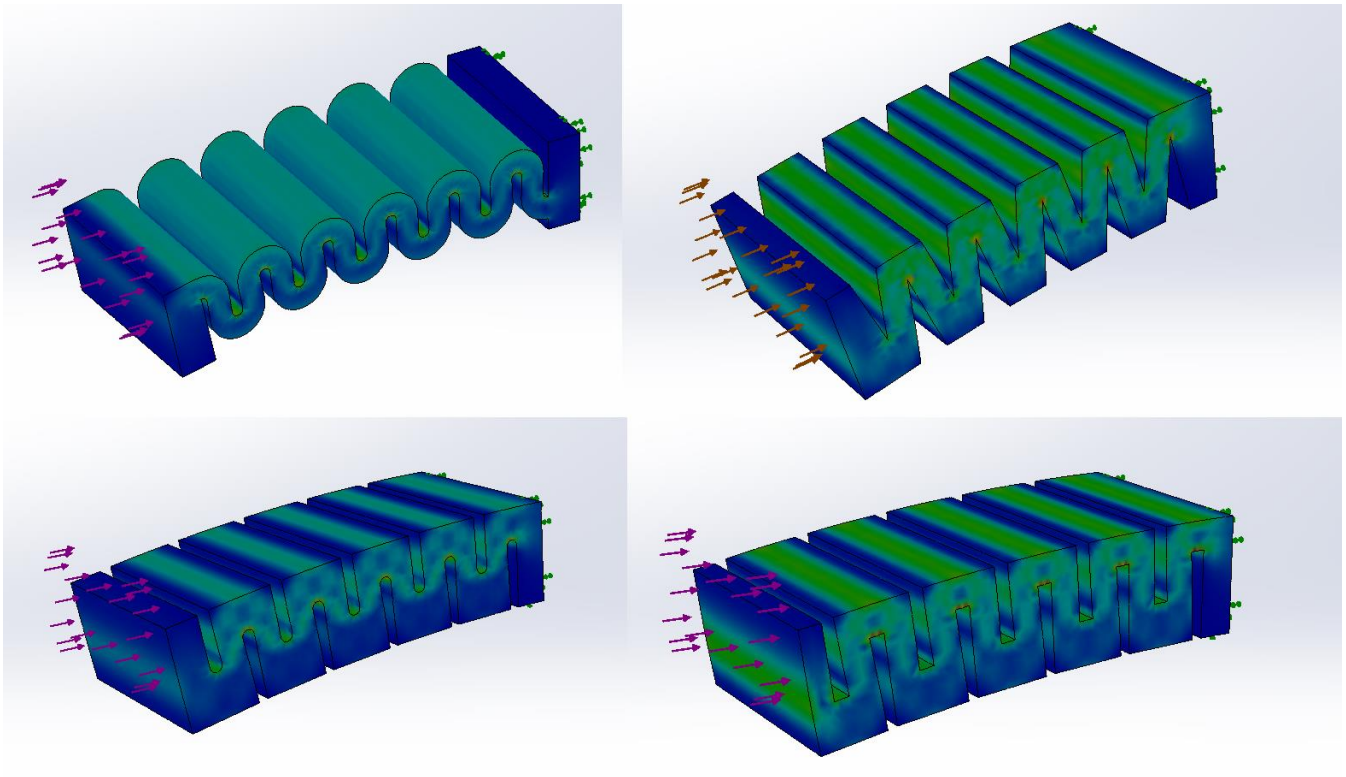

Figure D.3: Blocks after applying the force of 10 N. The lighter the color, the higher the stress on that specific area. (Stress-color ranges differ per geometry)

Table D: The results of the block tests for the rectangular, triangular, cylindrical, and wave geometries.

Geometry in block	Von Mises stress [MPa]	Factor of Safety
Rectangular	15.7	1.9
Triangular	11.5	2.6
Cylindrical	13.4	2.2
Wave	22.0	1.4

Appendix E: The effect of small changes in the pre-bent grasping mechanim.

In the Figure below (Fig. E.1 and E.2) practically the same structures are exposed to the same force. The only difference in the two figures is the amount of grooves. In Figure E.1 there are 14 small and 15 large grooves, while in Figure E.2, there are 11 small and 12 large grooves. These small changes have a large effect on the outcome of the simulations. The von Mises stress and the displacement obtained by the two grasping forceps structures are visible in Table E. However, the stresses might be different in quantity, the locations are still the same and both structures show the same stress concentration locations.

Table E: Von Mises stress and displacement obtained by grasping forceps with 14small/15large and 11small/12large grooves.

Number of grooves in geometry	Von Mises stress	Displacement
14small/15large	33.25 MPa	10.0 mm
11small/12large	21.80 MPa	5.56 mm

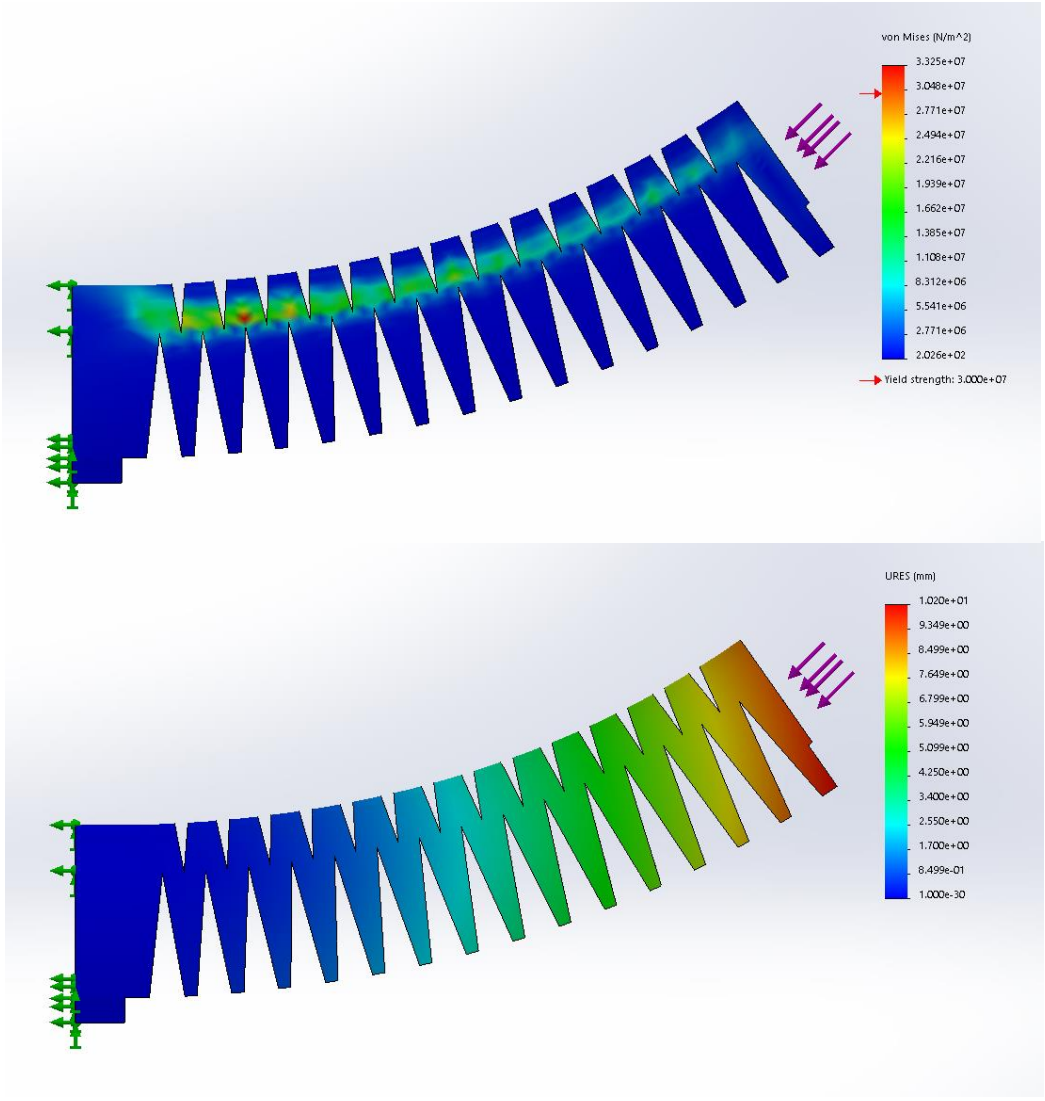

Figure E.1: Triangular pre-bent grasping forceps mechanism with on the top side 14 grooves with length 1.0 mm and on the bottom side 15 grooves with length 2.5 mm. Top image: von Mises stress simulation, bottom image: displacement simulation.

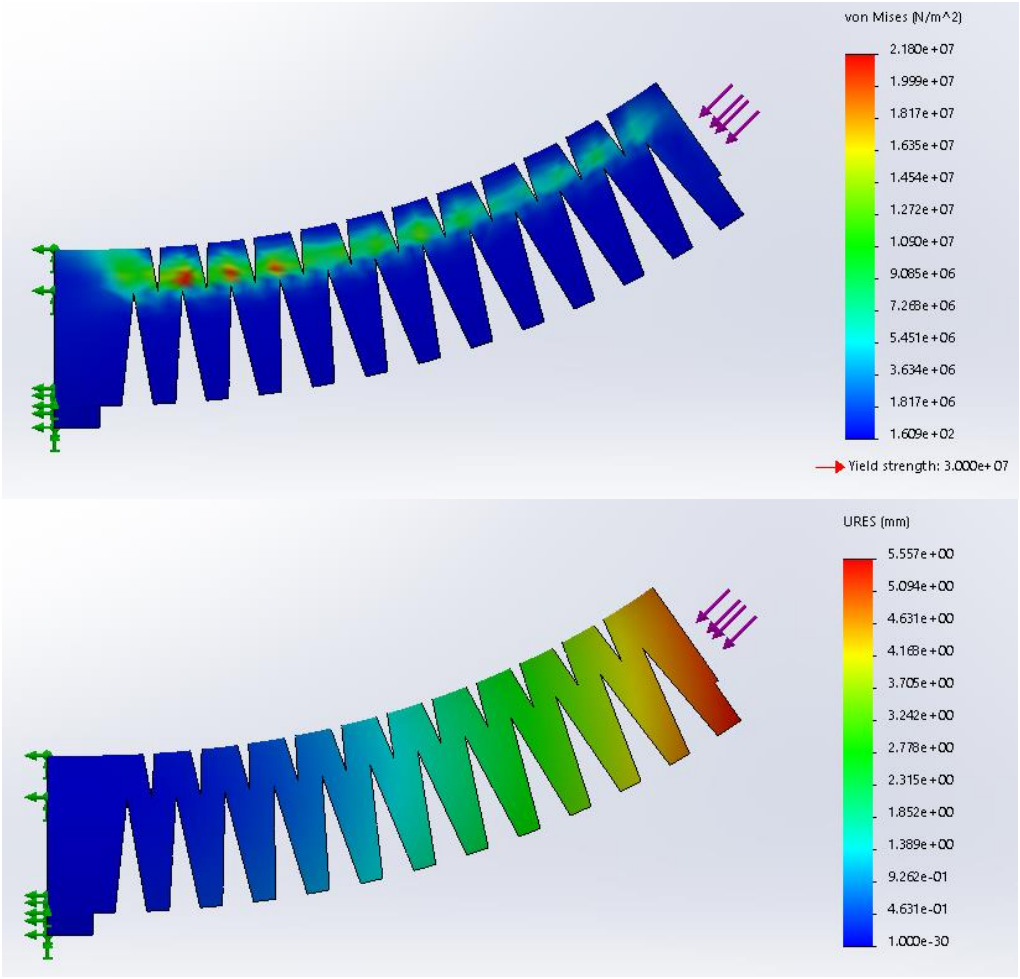

Figure E.2: Triangular pre-bent grasping forceps mechanism with on the top side 11 grooves with length 1.0 mm and on the bottom side 12 grooves with length 2.5 mm. Top image: von Mises stress simulation, bottom image: displacement simulation.

Appendix F: 3D image of grasping forceps with cable slots.

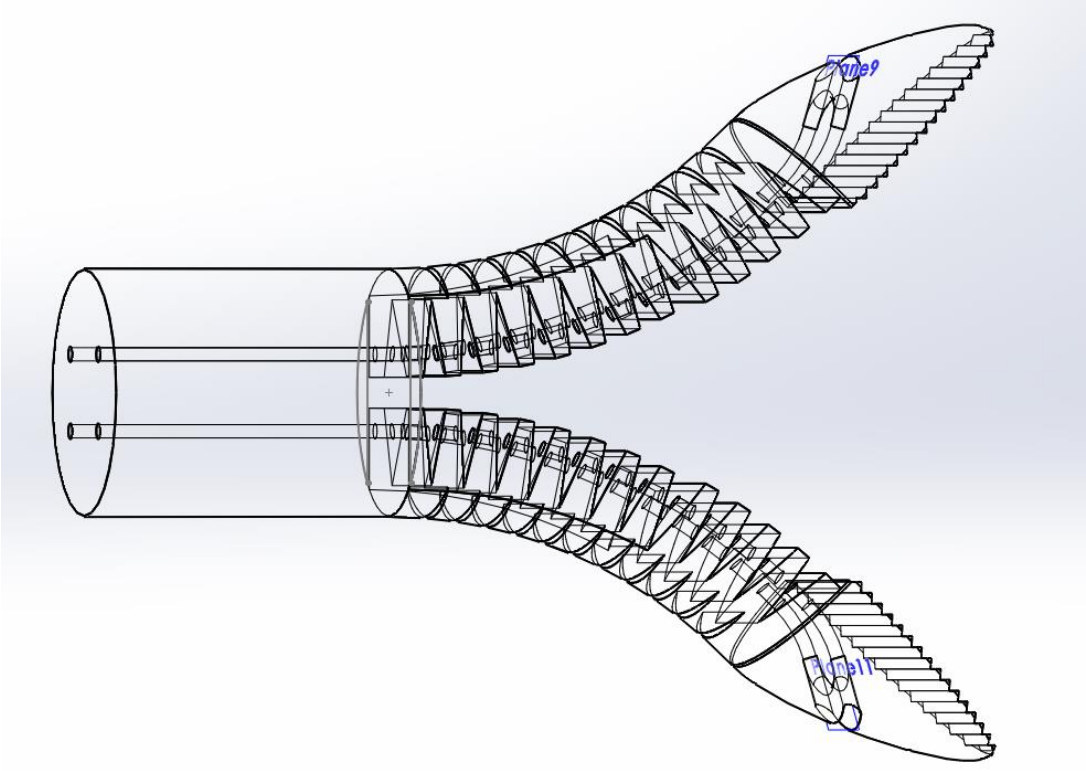

Figure F.1: See-through 3D image of part made in Iteration round I.

Appendix G: Close-up figures of control handle.

Figure G.1: Digital drawings of combined control handle halves.

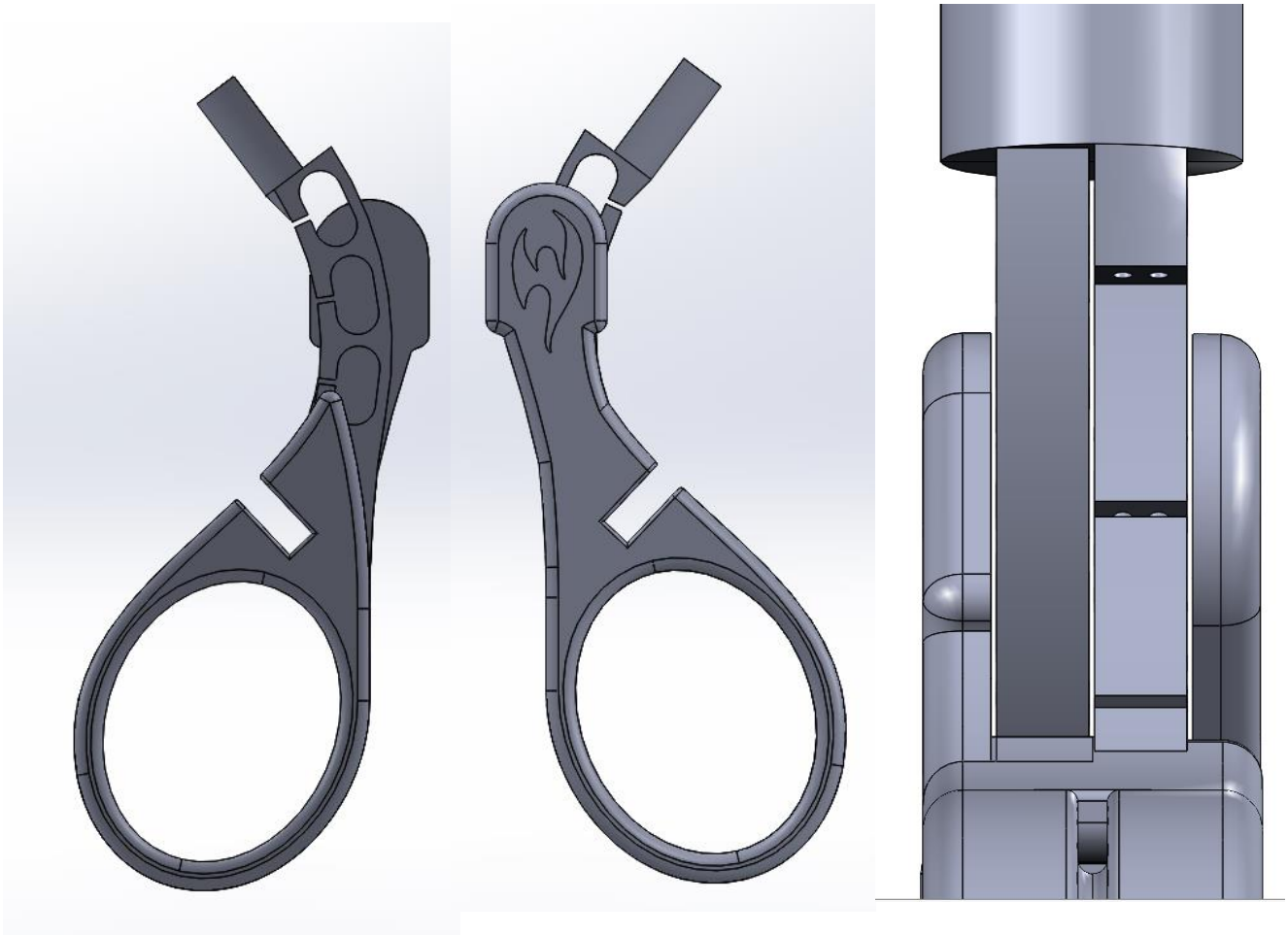

Figure G.2: Digital drawings of control handle halves: Left and middle: both sides of a control handle half, right: close-up of bending joint structures.

Appendix H: Calculations of maximum tensile stress withstand by MonoFlex.

Appendix H.1: Maximum tensile stress withstood by grasping forceps

The weakest area is in this case also the smallest/thinnest area of the grasping forceps. This is the thin layer of bending material on each grasping jaw. The area is calculated by integrating the function f(x) of the circle over the interval [3,4]:

$$\int_3^4 f(x)dx$$

With

$$f(x) = \sqrt{16 - x^2}$$

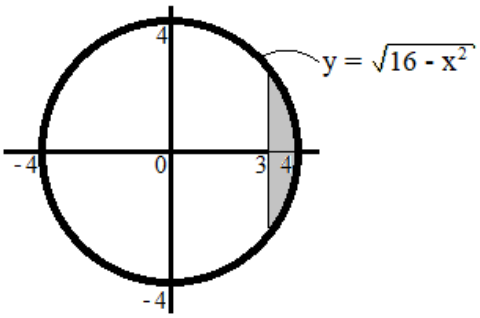

When solving this integral equation, an area of 1.8132 mm^2 is found. Since with this formula, only the top area of the circle segment is calculated, this value has to be doubled and becomes 3.6265 mm^2 for the complete segment.

The tensile strength of the material in theory is 30 MPa, which equals 30 N/mm^2. The maximum stress in theory, that could be withstand by the area of the circle segment, must therefore be 30 N/mm^2 · 3,6265 mm^2 = 108,79 N = 11,9 kg.

Appendix H.2: Maximum tensile stress withstood by control handle

The smallest cross section area at the control handle equals 1.0 mm · 2.5 mm = 2.5 mm^2. The maximum stress in theory, that could be withstand by the control handle, must therefore be 30 N/mm^2 · 2,5 mm^2 = 75,0 N = 7,65 kg.

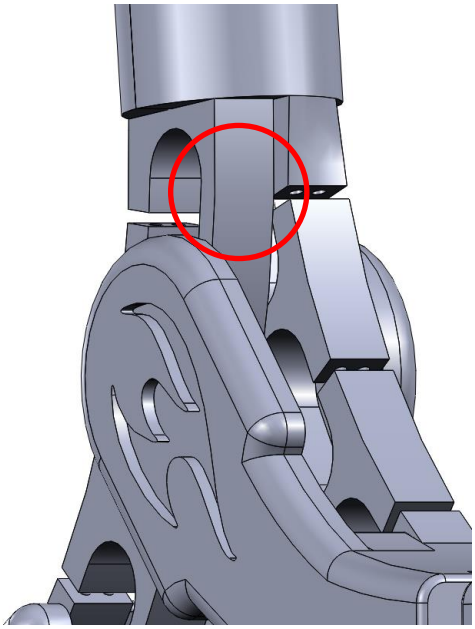

Figure H.1: Close-up of bending structure in control handle, red circle shows the critical spot.

Appendix I: Simulation of the compression test.

In Figure I.1, a simulation is visible obtained after applying two forces (purple arrows) in the direction of the arrows. Multiple simulations are performed, with different force magnitudes, until a factor of safety of 1.0 was reached. In this specific case, the stress has reached the maximum value before breaking the part. The factor of safety of 1.0 was found after applying a compression force of 0.6 N, which equals 61 gram.

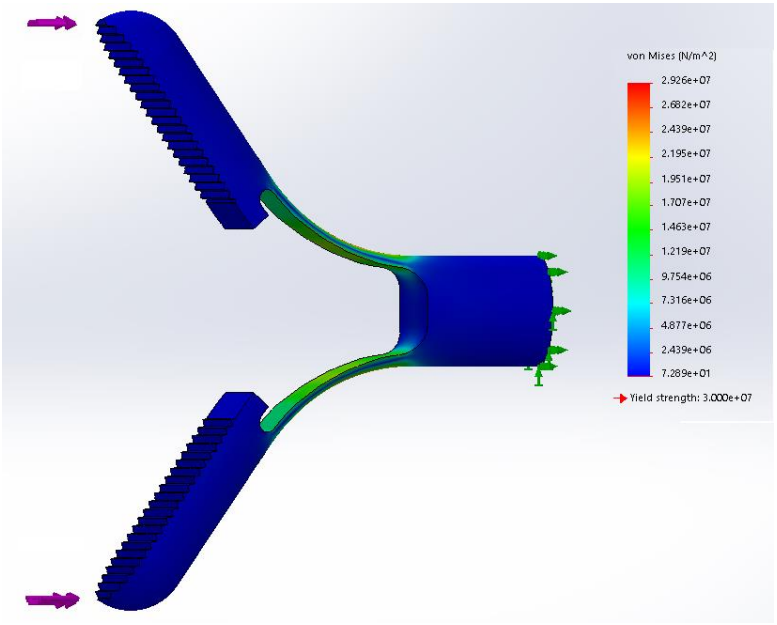

Figure I.1: Grasping forceps subjected to compressive forces of 0.6 N.